Accepted at *Quaternary Science Reviews*

# Distinguishing current effects in sediments delivered to the ocean by ice. I. Principles, methods and examples.

I. N. McCave[1] and J. T. Andrews[2]

[1] Godwin Laboratory for Palaeoclimate Research, Department of Earth Sciences, University of Cambridge, Downing Street, Cambridge CB2 3EQ, U.K.

[2] Department of Geological Sciences and INSTAAR, University of Colorado, Boulder, CO 80309, USA.

## Abstract.

There are climatically important ocean flow systems in high latitudes, for example the East and West Greenland and Labrador Currents and Nordic Sea overflows in the North, and Antarctic Circumpolar Current in the South, for which it would be useful to know history of flow strength. Most of the sediment records under these flows contain evidence of supply from glacial sources, which has led to the supposition that fine sediment records, which in other settings provide evidence of vigour of flow from the sortable silt proxy, are fatally contaminated by unsorted glacial silt. It is suggested here that if the fine fraction (< 63 μm) has been transported and sorted, then it does not matter that it may have been released from icebergs, sea ice or meltwater plumes. Here we show that correlation between sortable silt mean and percentage provides a good indicator of whether a fine sediment record has been sufficiently well current-sorted to provide a reliable flow history. The running downcore correlation ($r_{run}$) (5 to 9-point depending on sampling interval) is found to be optimal, and a value of $r_{run} < 0.5$ is proposed as an

indicator of sufficiently poor sorting to invalidate a section of mean size record. More than 40 grainsize records determined by laser particle sizers from over 30 core sites have been processed and examined for evidence of sorting. As expected, there is a tendency for poor sorting and unreliable records at points where the flow speed has decreased to very low values. There is no consistent relationship between the sorting of the fine fraction and the content of coarse ice-rafted debris (as long as the IRD fraction is not > 50%) because the two are not related. End member (EM) decomposition of several records yields variable results in terms of the relationship between EM ratios and grainsize parameters. Although such an approach can generate fine sediment parameters it does not provide a basis for deciding whether or not a record is acceptably current sorted and thus contains a valid flow speed proxy. Our proposed discrimination between current-sorted and unsorted fine fractions is applicable to all fine grained deposits, not only high-latitude deposits with coarse IRD.

Examples from East Greenland, Faroe Bank Channel, Gardar Drift show mainly well sorted signatures. Amounts of coarse IRD range up to 60% with only those >50% having a consistent impact on sortable silt mean size. With the exception of a Southern Ocean site on the Antarctic continental rise where half the record is poorly sorted, the silt mean data are sufficiently well sorted to provide credible flow speed histories. This bodes well for the extraction of such histories from climatically important high-latitude flows such as the East Greenland Current.

KEYWORDS: Ice-rafting, sortable silt, fine sediment, laser sizers, downcore correlation, East Greenland Current, Labrador Current, ice-rafted debris, IRD, End Member.

# 1. Introduction.

Sedimentary records located in high latitudes frequently originate from glacial sources either from ice rafted debris (IRD) or meltwater plumes ( Syvitski, 1988; Stein, 2008; Hudson et al., 2014). However, these records may also contain evidence for the changing vigour of both deep and shallow components of the ocean circulation. Such sedimentary flow records, based on properties of the fine fraction (<63 μm), are frequently viewed with suspicion because they contain abundant evidence, particularly in the form of coarse sand and gravel sized components, for delivery by ice rafting. The suspicion is that the sediment on which such records are based has not been sorted by a current. For example Jonkers et al. (2015) remark "*Since ice-rafted detritus (IRD) is not limited to coarse particles only, IRD input can lead to changes in the mean silt size and hence spuriously suggest current speed changes. .... regions and/or times with IRD input are generally avoided*.", and Wu et al. (2018) say "*In polar oceans, the ''sortable silt'' fraction, however, is in many cases a mixture of material supplied by bottom currents and icebergs...*". However, we argue that, if the fine fraction (< 63 μm) has been transported and sorted, then it does not matter that it may have been released from icebergs, sea ice or meltwater plumes, and is unrelated to the associated coarse fraction (Figure 1A). This is because the coarse fraction is essentially immobile (the critical geostrophic erosion velocity of medium sand (d >250 μm, $U_g \gtrsim 45$ cm $s^{-1}$) is a speed that is rarely achieved for sustained periods in the deep ocean). If this size were to be frequently moved a sandy lag deposit would result with minimal fine fraction and often with dune bedforms (Flemming, 1978). If, however, ice rafting delivers fine and coarse material into a sluggish current then the

fine fraction is unlikely to be sorted and coarse and fine fractions are indeed associated genetically (Figure 1B).

Given these scenarios (Fig. 1) we therefore seek a way of detecting whether a given sediment record of the fine fraction that contains IRD, or part of such a record, has not been current sorted and is therefore unreliable as evidence for changing vigour of the ocean circulation and its relation to climatic variables. Upon detection of unreliable sections the data could be simply removed from a time series, leaving credible data of flow history, in place. This paper argues that the degree of correlation between the Sortable Silt (SS) mean size ($\overline{SS}$) and percentage (SS%) in the fine fraction provides an index of sorting (McCave et al., 1995; McCave & Hall, 2006) and contains a criterion for rejecting or accepting parts of downcore records as indicative of flow speed history. The common measures of sorting based on properties of the normal distribution (standard deviation and graphical equivalents, e.g. Inman, 1952; Folk & Ward, 1957) primarily work for sands and are not applicable here in silt distributions truncated at 10 and 63 μm. Correlation with amount of coarse IRD is deemed to be irrelevant to making this distinction, and End Member modelling ( e.g. Jonkers et al, 2015; Wu et al., 2018) merely provide statistical associations of no utility in solving this problem (see section *4.4*).

### *1.1 Questions.*

Consider the following two situations:

First, sea ice or icebergs melt releasing glacially derived (i.e. till) sediment which settles through the water column to the bed where a current is intermittently strong enough to pick up and transport the fine fraction of the released sediment, but

it is not strong enough to transport the coarser sizes (i.e. material >150, >250 or >500 μm, critical geostrophic erosion velocities are ~40, ~45 and ~55 cm $s^{-1}$, based on Miller et al. (1977)). In such a case the coarse material stays more or less beneath the point at which it was released from ice, whereas the associated fine material may have been released some considerable distance upstream (Fig. 1A). In this case the fine fraction will have size distribution characteristics reflecting the strength of the current performing the sorting during transport and deposition. The presence of coarse ice rafted detrius (IRD), being genetically unrelated, does not then indicate absence of current sorting of the fine fraction.

In the second case the sediment released from icebergs or sea ice falls into a sluggish flow which, while moving sediment a short distance as it falls through the water column, does not resuspend and transport either the fine or coarse fraction (Fig. 1B). In this case the size distribution characteristics of the fine fraction are essentially those of the glacially eroded sediment contained in icebergs or coastal/shallow shelf sediments incorporated in sea ice. Data presented by Andrews and Principato (2002) show that this material contains a large amount of coarse and/or fine silt, so the presence of unsorted IRD may not be presumed to yield either a coarser or a finer sortable silt (SS) fraction (10-63 μm), but it does confound any interpretation in terms of flow speed. Sea ice transport can be long distance, originating from shoreline and inner shelf sediments, some of which may be well sorted.

We then pose the following questions: 1) **Is there a parameter or a set of parameters that distinguishes current-sorted from unsorted fine sediment**

**originally introduced by ice rafting?** In a well current-sorted deposit cross plots of the sortable silt mean size $\overline{SS}$ (μm) and percentage (SS%) display a close relationship (McCave et al., 1995; McCave & Hall, 2006; McCave et al., 2017). So, question 2): **Can plots of $\overline{SS}$ vs SS% be used to identify data for which current sorting has been ineffective**, i.e. to recognise a sortable silt mean size ($\overline{SS}$) record which may **not** be interpreted as reflecting varying flow speed.

In order to examine these problems a number of cores containing IRD have been investigated and analysed by laser diffraction particle sizing methods capable of giving broad spectrum (< 1 to > 1000 μm) sediment grain size analyses. These have been taken from published works ( Table 1 'Core Locations') and some of our unpublished data.

*1.2. Some problems of glacial-marine sedimentation in relation to our core sites*

Ice-proximal to ice distal glacial marine cores sites (Table 1) were obtained from outer shelves and deep glacial troughs rather than deep-sea sediment basins. Such sites frequently have complicated lithofacies and grain-size changes linked to changes in glacier extent, presence/absence of an ice shelf or pervasive sea ice, and ocean climate. Icebergs often deliver glacial tills, which, in general, have a large fraction of their grain-size <63 μm (Dreimanis, 1976, 1979; Drewry, 1986). However, most working definitions of IRD among marine sedimentologists focus on the sand or larger fractions even though it is often a minor component (Andrews, 2000) and little attention has been given to the ice rafting transport of <63 μm sediments, except for purposes of sediment transport and provenance (e.g. Verplanck et al., 2009; Andrews, 2011). In extreme ice proximal locations, such as under a former ice shelf

(McKay et al., 2016; Jennings et al., in press) or in areas of landfast sea ice, coarse IRD is absent and the sediments are often laminated silty clays or clayey silts ( Reeh et al., 1999; Dowdeswell et al., 2000; Reeh, 2004). Also "glacial" sediments (primarily silts and clays) can be transported tens to many hundreds of km from the ice margin in meltwater plumes (e.g. Andrews and Syvitski, 1994; Syvitski et al., 1996; deGelleke et al., 2014).

Sea ice transport Sea ice transport originates from coastal locations (Barnes et al., 1982; Nürnberg et al., 1993), although not much makes it to East Greenland in Demnmark Strait where the mineral composition of Holocene sediments show limited contributions from sites around the Arctic Basin (Darby et al., 2017), and the sediment is dominated by contributions from the glacial erosion of the East Greenland flood basalts (Andrews et al., 2015) with limited export of felsic-rich sediments from NE Greenland (Andrews and Vogt, 2014). Sediment may be incorporated in sea ice by freezing on at the shoreline and by freezing onto the bottom of sea ice from wave resuspension at the inner shelf (Dethleff & Kuhlmann, 2009). The shoreline sediments are mainly sands and gravels some of which will be well sorted, while the resuspended inner shelf sediments may contain fine material, some well sorted. This material will suffer the same fate as that released from icebergs or meltwater plumes when close to the bed by either being deposited directly with no further resuspension under weak flow or, under a current, being resuspended and sorted further downstream. Well sorted fines dropped into a slow flow from sea ice could cause problems if not diluted by unsorted material from icebergs.

## 2. Materials and Methods

### *2.1. Core grainsize database*

We have assembled a database of laser particle size determinations on about 40 cores from high latitudes, including a few terrestrial sections and a suite of surface samples ( Table 1). Most of the marine cores are from ice-influenced latitudes with a particular focus on locations to the east and west of Greenland. All of the marine sections are influenced by the input of ice-rafted coarse and fine material. Some of the sample preparation follows the protocol of McCave et al. (1995) in removal of carbonate (and opal). This was to remove biogenic influences of foraminifera, coccoliths and diatoms. These procedures have not been followed in the majority of the data used here because most high latitude sediment delivered by ice/glacial processes contains little such material and carbonate grains comprise an important fraction of glacially derived sediment originating from the erosion of limestone and dolomite, such as noted in Hudson Strait Heinrich events (Andrews and Voelker, 2018) or in Baffin Bay detrital carbonate events (Jennings et al., 2017).

### *2.2. Use of laser sizer data.*

Although one of us is on record criticising the use of laser sizers in the determination of fine particle size on the grounds of shape effects (slow sinking platey particles) below 10 μm that leak into the >10 μm range (McCave et al., 2006), convincing laser results have been presented by Piper and his associates (Marshall et al., 2014; Li & Piper, 2015; Mao et al., 2018). In particular, Marshall et al. point out

that glacial sediments are likely to resemble the crushed quartz material for which Konert and Vandenberghe (1997) detected no significant shape effect. Thus laser sizer data are used here. The advantage of the laser sizer is that it covers a very wide size spectrum from < 0.5 μm to 2 mm or greater encompassing both the SS range and sand-sized IRD.

The parameters sortable silt mean size ($\overline{SS}$) and percentage (SS%) were obtained from grainsize analyses of the selected samples (McCave et al., 1995). There is now a calibration of $\overline{SS}$ in terms of sensitivity of size to speed, i.e. the change in speed can be deduced from a change in $\overline{SS}$ size (McCave et al., 2017). That calibration is expressed in terms of size measured by Sedigraph and Coulter counter between which McCave et al. (2017) give a good intercalibration relationship ($\overline{SS}_{sedi}$ = 0.926 $\overline{SS}_{cc}$ - 0.95; r = 0.968). No satisfactory relationship has been available between a laser and the other instruments. An initial objective was to provide one.

Some samples from JM96-1206 have also been measured using a Coulter counter (Coulter Mastersizer Mark 3). A comparable dataset was also created by Jonkers et al. (2015) who used a Fritsch A33 laser and the same model of Coulter counter. At the time of the calibration paper of McCave et al. (2017) there was only that dataset available for a counter-laser relationship which had a rather low correlation coefficient ($r$ = 0.548). Combining the two data sets gives a result with the Reduced Major Axis (RMA, Miller and Kahn, 1966) slope of 0.946 ($\overline{SS}_{las}$ = 0.946* $\overline{SS}_{CC}$ + 1.68) and a correlation coefficient coefficient of 0.812 (Supplementary Information #2). As the sensitivity for the Coulter Counter is 1.26 cm $s^{-1}$/μm this

preliminary result implies a sensitivity for the Fritch and Malvern lasers of 1.33 cm $s^{-1}$/μm. Where flow speed changes are given below this is the value applied to $\overline{SS}$ differences.

If IRD sand sizes are present, laser sizer data allow extraction of the percentage of IRD in several size fractions. Commonly used is the >150 μm fraction because this is used for the analysis of foraminifera. However, it is not an ideal size because its critical erosion velocity is rather close to the critical erosion velocity of the coarse end of the silt spectrum. However some datasets show that the > 250 μm fraction correlates very well with the > 150 μm fraction (e.g. JM96-1206, r = 0.968). Although the >500 μm fraction is preferable on dynamical grounds there is frequently so little material of that size that the results show considerable scatter. Wherever the data permit it we have used the ≳250 μm fraction in this paper.

*2.2.1. Processing scheme*. The raw laser data commonly do not contain bin edges at 10 and 63 μm so these sizes are inserted in the spreadsheet and interpolated percentages from the bin that straddles the boundary are entered. The sortable silt mean size is calculated using the 'sumproduct' function in Excel on the percentages in bins multiplied by the natural log of the bins' geometric mid-point diameters. The exponential of this product divided by the sum of the percentages between 10 and 63 μm gives the sortable silt mean size $\overline{SS}$ (mean between 10 and 63 μm) (Blott and Pye, 2001) (see examples in Supplementary Information #1). The sortable silt percentage (SS%) is calculated as the sum between 10 and 63 μm divided by the total fine fraction (% <63 μm). Running correlations between the $\overline{SS}$ and SS% downcore are then calculated, mainly in 7- or 9-point windows (see section 3.4 for

justification/discussion). Several coarse fraction percentages can represent IRD (>150, >250, >500 μm, (2¾, 2, 1 φ)) depending on the presence of the material in the data. For some datasets close equivalents, e.g. 240/257,497/ 516 μm, are used because interpolation would make negligible difference. (In what follows the notation IRD followed by a number signifies the percentage greater than that size in the whole distribution up to 2 mm, e.g. IRD250 is the percentage > 250 μm.)

*2.2.2. End Member decomposition.* In a few cases we have tested an End Member (EM) decomposition to compare with results obtained by the originators of some data sets (Jonkers et al., 2015; Wu et al., 2018). The EMs are deduced from a statistical procedure analogous to principal component analysis (Weltje, 1997; Seidel & Hlawitschka, 2015; Paterson & Heslop, 2016) and we have used the Paterson & Heslop scheme here.

## 3. Establishment of a fine sediment sorting index

### *3.1. Surface sample data from cruise HU 70037, W. Baffin Bay*

This suite of surface sediments on the shelf off W. Greenland under the West Greenland Current (WGC) is used to show how the method works. It shows excellent sorting with a correlation coefficient between $\overline{SS}$ and SS% of r = 0.961 (n = 56) (Fig. 2A). Andrews et al (2018) identify several grainsize clusters some of which have a significant coarse mode of IRD240. Removing these 11 samples from the data plot does not significantly increase the correlation: it rises from 0.961 to 0.964. The correlation between $\overline{SS}$ and % IRD240 is not strong (r = 0.56, Fig. 2B) and thus *there is no evidence that the silt mean size is controlled by a process related to input of coarse IRD*. We conclude that the fine fraction is well sorted by the current, and downcore

sortable silt fractions from this area could be interpreted in terms of variation in the WGC.

### *3.2. SS parameters of diamicts*

To check whether sediments show a poorly correlated relationship between $\overline{SS}$ and SS% where current influence is not suspected, we have assembled over 50 analyses of basal diamicts encountered in several cores (Fig. 3). For the diamicts the plot of $\overline{SS}$ versus SS% shows no significant relationship (Fig. 3A) and $\overline{SS}$ versus % IRD240 is not strong ($r = 0.583$; Fig. 3B). Thus, as expected, these diamicts show no evidence of sorting of the fine fraction. However, it is worth noting that it is sediments like these that are transported by icebergs and which contribute both coarse IRD and silts and clays to distal sediment deposits. Some basal units contain shell fragments and foraminifera. It is possible that these represent glacially overrun proximal glacial marine deposits. Samples in this category showing a high SS-SS% correlation have not been included in Fig. 3.

### *3.3. SS parameters of terrestrial (lake, delta) sediments deposited from water*

Sediments from receiving basins on the Mississippi Delta top (data from Xu et al., 2016) also show no sorted relationship between $\overline{SS}$ and SS%. Material is rapidly introduced from overflows which do not appear to sort the fine fraction (Fig. 4A). A similar situation seems to occur at Alberta Lake E (data from Gammon et al., 2017), where two clouds of unsorted fines occupy space in an $\overline{SS}$ versus SS% plot (Fig. 4B), but a third group with SS% > 60% shows a linear relationship suggesting current

sorting. The latter data occupy two discrete sections of the core with high 'D3 mode' area in Gammon's analysis, suggesting periods of sediment-sorting flow.

### 3.4 *SS parameters of terrestrial (loess) sediments deposited from air*

A deglacial to Holocene downcore record of grainsize from the Chinese Tien Shan Mountains has been published by Jia et al. (2018). These windblown silts, which fall mainly in the sortable silt grainsize range, have an overall $\overline{SS}$-SS% correlation coefficient of r = 0.776. This may not seem high, but the section contains several palaeosols which may affect the wind-blown size signature (Chen et al, 2016)

### 3.5. *Use of moving downcore correlation between* $\overline{SS}$ *and SS%*

From the foregoing arguments and data we conclude that the correlation between $\overline{SS}$ and SS% provides a useful indicator of sorting in the non-cohesive medium to coarse silt fraction (10-63 μm) of fine sediments. As previously demonstrated, the mean size ($\overline{SS}$) is an indicator of the speed of the depositing flow (McCave et al., 2017). The plot shown in Fig. 2A is derived from a spatial array, but similar plots may be obtained from a temporal array, i.e. a plot of samples taken along a core. Such an array may be partitioned into segments showing a high degree of correlation (well sorted), and those with low correlation that put in doubt the sorting of the silt by its depositing flow. In the latter case we should not use parts of the $\overline{SS}$ record with 'too low' correlation. To evaluate intervals where changes in the SS parameters are occuring we use a running downcore correlation coefficient ($r_{run}$) on a window of 5, 7 or 9 points. There is a trade-off here inasmuch as a longer run of

points, although smoother, encompasses a longer time period and may not be sensitive to significant short period fluctuations, e.g. Heinrich Events. In Fig. 5 the 13 point is clearly too smooth but the 5 point has much short period variability. The 7 and 9 point runs capture the major features. However, this latter window is ~ 9.7 ka in MD99-2323 and this may be thought too coarse. The length of run selected will therefore depend on the length and sampling resolution of a record.

It is important to ask: How low is 'too low' for $r_{run}$ , i.e. at what level can part of a record not be relied upon to yield credible values of $\overline{SS}$. Initially we considered using $r_{run}$ = 0.7 as the criterion. Examination of many records shows this to be quite conservative and that 0.5 is satisfactory. Figure 6 shows data for MD99-2323, a core from the Snorri Drift (Fig. 2) (Dunhill, 2005; Dunhill et al., in prep) where the blue highlights mark sections where the 9-point correlation coefficient $r_{run}$ is below 0.5, removing periods of 123-108 ka in Marine Isotope Stage (MIS) 5 and the last 13 ka, with a few other minor excursions, for which the validity of the sortable silt mean as a recorder of flow speed would be in doubt. Relevant correlation coefficients are 0.773 for $r_{run}$ >0.7, 0.765 for $r_{run}$ >0.6 and 0.770 for $r_{run}$ >0.5, so a value of 0.5 is acceptable here. There is no obvious correspondance to be seen in Fig. 6 between $r_{run}$ and IRD257% save at 108-123 ka.

An alternative to the running correlation coefficient is the absoute residual distance of a point from the best fit line for the array. Distances from RMA or linear regression fits give similar results (they are correlated at r = 0.93). To use the Absolute Residual or difference from RMA as a discriminator for downcore runs requires setting a value for acceptability, as with $r_{run}$. Regions of greater distance

from the line, if not random, might have been expected to correspond to lower $r_{run}$. However for neither measure is there agreement with the running correlation coefficient (see Supplementary Information #3 ), so this method has not been adopted

The default setting is thus a 5 or 7-point running correlation for short data sets (< ~50) and 7 or 9-point for longer ones, with $r_{run} < 0.5$ marking sufficiently poor sorting to make $\overline{SS}$ values unacceptable as flow speed indicators.

*3.6 Slope vs Intercept*

The plots of $\overline{SS}$ vs SS% with RMA fits (line passes through the respective mean values) are characterised by a slope and an $\overline{SS}$ intercept at SS% = 0. The intercepts decrease with increasing slopes of the plots of $\overline{SS}$ vs SS% as is expected given the fairly narrow range of mean values of the variables (Fig. 7), providing a possible index of the efficiency of sorting. There is a poor relationship of slopes to flow speed proxies, making it a weak proxy for the efficiency of fine sediment sorting.

*3.7 Slope vs Correlation*

An additional consideration is that the slope of the $\overline{SS}$ – SS% relationship be positive and higher than some value. The lowest slope in our data sets is 0.0708 for a group of points which have r = 0.812 from glacial terminations in a core at the Antarctic continental rise (see section 4.4 below). With a slope lower than this it would be difficult to maintain that the sediment was sorted (noting that a slope of zero has a correlation of zero). A requirement that slope be ≥ 0.70 is suggested (Fig. 8).

## 4 Examples of Applications

We have analysed the laser data for >3100 analyses from 32 cores (Table 1) and one terrestrial loess section. The results given in Table 2 and Fig. 7B show that the great majority of the records have overall $\overline{SS}$ - SS% correlation coefficients >0.80.

A few examples of the use of the running correlation discriminator are given for high latitude cores influenced by IRD from E. Greenland, Faroe BankChannel and distal Iceland-Scotland Overflow (Gardar Drift) as well as the Antarctic record of Wu et al. (2018) off Prydz Bay. Further examples and their palaeoceanographic and palaeoclimatic significance are presented in a companion paper (McCave and Andrews, in prep).

### 4.1. *East Greenland: High quality records with moderate coarse IRD percentage*

There are several records of high quality from East Greenland and Northwest Iceland for the Holocene shown in Fig. 9. These contain relatively few periods with unacceptable $\overline{SS}$ data, and the major features of the records from East Greenland (JM96-1210 & -1206) documenting the East Greenland Current display the same trends. The $\overline{SS}$ vs SS% plots display excellent to good sorting ( $r_{run}$ = 0.923 (JM96-1206), $r_{run}$ = 0.805 (JM96-1210)), and in the case of MD99-2269 from NW Iceland two distinct parallel lines are evident, each with a correlation coefficient > 0.96 and occupying two distinct depths in the core (age boundary at 9.2 ka) (Fig. 9 inset). A change in provenance with a coarser supply during deglaciation and rising sea level is a possible explanation. The fact that the sensitivity of differences to flow speed

changes is calibrated (McCave et al., 2017) means that the two provenances can still be converted into flow speed changes. These are an increase of 6.3 cm $s^{-1}$ from 11 to 9.2 ka and a decline of 9.3 cm $s^{-1}$ from 9 ka to the present of the N. Iceland Irminger Current. The percentages of IRD250 are low to significant, ( 0 - 3.8% in JM96-1206, 0.7 - 17.1% in JM96-1210, and 0 – 1.4% in MD99-2269) but have little influence on the sortable silt mean sizes (respective correlations are 0.454, 0.119, 0.038).

The Holocene climatic optimum between 9 and 7 ka, delayed around Iceland due to the impact of freshwater from the melting northern Laurentide Ice Sheet (LIS) (Jennings et al., 2011) ---water supplied via the Arctic Ocean and Fram Strait, is marked by a flow speed maximum between 9 and 7 ka (including a sharp decrease in MD99-2269 at the time of the 8.2 ka event) and a steady decline in flow speed from 7 to 4 ka at NW Iceland, and 7 ka to the present in the other records. Flow speed minima are apparent around the time of the 3.2 to 2.7 ka and 4.2 ka cold/dry events (Wanner et al., 2011; Supplementary information #9). These surface currents behave congruently with terrestrial climate and the deep overflows in the Iceland Basin recorded by Hoogakker et al. (2011; Supplementary information #8). The records demonstrate that high quality flow speed records can be obtained from deposits with a high percentage of coarse IRD.

*4.2. Faroe Bank Channel: Acceptable* $\overline{\text{SS}}$ *with very high IRD percentage.*

Data from Faroe Bank Channel (GC083, McIntyre and Howe, 2009) are remarkable in that the fine fraction is well sorted (r = 0.86) but the sediment contains very large amounts of coarse IRD, (IRD257 up to 60% in the fraction <2 mm) (Figs. 10 & 11). The large amounts of IRD occurring between ~40 and 34 ka do not appear to

have an effect on the mean size but the values over 50% in the Holocene are mostly accompanied by correlation coefficients of < 0.5 making the data that suggests a reduction in flow speed through the Holocene unreliable. Present-day flows through Faroe Bank Channel are high-speed and the unreliability of the record must be due to the very high coarse IRD content (>50%) rather than inability of the strong flow to sort sediment.

We suspect that the region in Fig. 10 displaying greater scatter where SS >28 μm and SS% is >50% is related to the fact that at high speed the amount of sand in relation to fine material increases. That is because the fine sediment is frequently resuspended and dispatched to deposition at sites farther downstream where the flow is slower. The higher sand content results in the 'hiding effect' coming into play in which fine grains are trapped in between the coarser ones (e.g. Nino et al, 2005). This could result in the accumulation of relatively unsorted fines leading to greater scatter in the meanSS versus SS% plot. The fact that under high speeds the sorting effect appears to extend beyond the sand- silt boundary at 63 μm has also been noted by other workers including Lamy et al. (2015) under the Antarctic Circumpolar Current (ACC) as well as Li and Piper (2015).

The flow history suggests flow speed oscillations of a few ka in duration through isotope stage 3 and a significant hiatus through the deglaciation probably caused by high velocities in the early Holocene and possibly also in the Bølling-Allerød. The acceptable parts of the Holocene record indicate flow speeds significantly greater (by at least 10 cm $s^{-1}$) than those in stage 3.

*4.3 Gardar Drift: Moderate IRD content and EM decomposition*

ODP Site 983 has been the subject of several studies including that of Kleiven et al. (2011) who showed a close relationship between $\overline{SS}$ and $\delta^{18}O$ of both planktonic and benthic foraminifera with low $\overline{SS}$ during cold periods in MIS 18-22. Examination of laser size data from the period 10 to 35 ka by Jonkers et al. (2015), using an end member decomposition, suggested that EM models would allow recognition of contamination of a sortable silt record by IRD and elimination of its effects. They noted a similar timeseries pattern between coarser $\overline{SS}$ and high values of IRD150 percentage and suggested that some of the silt fraction was also of IRD origin during coarse IRD events. It is not clear how an EM ratio could make the distinction between ice rafted silt and current transported silt in a deposit under current influence, because, if there is a strong enough flow, both are current-transported. The key must be to decide whether or not the fine fraction is well sorted, not the simple presence of fine or coarse IRD. The plot of these data with the $\overline{SS}$-SS% 9-point correlation coefficient suggests that some of the peaks in IRD150 are indeed associated with poor sorting of the fine fraction but some are not, for example the period 18 to 14 ka (Fig. 12). (The 9-point window is mid-point ± 1.25 ka wide.). The IRD indicator EM3 is correlated with SS% at r = 0.992 (Fig. 13D).

The ratio EM2/EM1 proposed as a flow speed indicator by Jonkers et al. (2015) shows no relation to $\overline{SS}$. (Surprisingly the ratio (EM2/(EM2 + EM1) proposed by Wu et al. (2018) (but determined by a different program for a different data set) shows an excellent correlation with $\overline{SS}$ (r = 0.956), Fig. 13. This is somewhat ironic in

that this ratio does not correspond well with $\overline{SS}$ in their own dataset.). In the ODP 983 data from MIS 18-22 (Kleiven et al., 2011) most poor correlations occur in glacials, stadials or cooling episodes, suggesting that the slower flow was not capable of sorting the fine fraction introduced at high rate during those times (Supplementary Information #4). However, during the last glacial maximum (LGM) the flow was slow (low $\overline{SS}$) and sorting is good.

*4.4. Prydz Bay, ANT30/P1-02, (Wu et al., 2018); poorly sorted fines with low coarse IRD*

A long record with several influences that poses difficulties is that of ANT30/P1-02 at 2916 m depth on the Antarctic continental rise 250 km north of the Prydz Bay shelf edge. For the full data set $r_{run}$ = 0.462 (312 points) indicating that much of the record is poorly sorted and $\overline{SS}$ is a dubious current speed recorder overall. It may be that there are source differences contributing to scatter because the cross plot of the high correlation data ($r_{run}$ > 0.9) displays two clusters of points separated at SS% ≈ 25 with an overall correlation coefficient of 0.839 (where it ought to be > 0.9 for a homogeneous population) (Fig. 14A). When the data with $r_{run}$ > 0.8 is added the correlation is still only 0.719. As will be seen later, parts of the data are well sorted but fall into two groups (Fig. 14B).

The downcore record with a 9 point running correlation suggests that only about 50% of the record has acceptable sorting for a flow speed recorder (Fig 15). The record displays several interesting features, notably that all of the glacial terminations have high correlations suggesting that a current is active in the transition from glacial to interglacial (Fig 15). However, the $\overline{SS}$ values do not

increase during these terminations. Correlation remains high in MIS 12, MIS 9-early 8, MIS 6 and part of MIS 3, primarily glacials and mostly recording high speeds declining to low going into full glacial conditions (e.g. MIS 13 to 12, 11 to 10, 9 to 8 and 3 to 2).

$\overline{SS}$ vs SS% for the transitions sorts into two groups displaying tight relationships with differing slopes. These comprise termination IIIa , V and 'VIa' (actually the transition between MIS 13b and 13a), and the early Holocene plus terminations II and III (Fig. 14B). This difference may reflect some change in the material delivered to the site, further evidence for a possible source change. The blue bars in Figure 15 denote the regions with invalid flow speed parameters. However the possibility of a source effect does introduce an added layer of complexity. Although the amount of coarse IRD is very small (only 9 points with IRD177 > 2%) and the correlation between $\overline{SS}$ and IRD147 is only 0.293, there is probably a significant amount of fine IRD.

The data were analysed by Wu et al (2018) using a 3 EM decomposition (Seidel & Hlawitschka, 2015) from which they deduced a current indicator given by the ratio EM2/(EM1+ EM2). We re-calculated the EMs (Paterson & Heslop, 2015) (Fig. 16A) and show that this ratio has a near perfect correlation with SS% (r = 0.988) (Fig. 16B) but poor correlation with $\overline{SS}$ (r = 0.356) (Fig. 16C) thus casting doubt on its suitability as a current speed indicator. SS% may also reflect the input of silt but, to the extent that SS% is also a flow recorder, the EM ratio also indicates activity of a current at this site during all terminations (Fig. 6 in Wu et al.). Nevertheless, if the silt fraction is not current-sorted it is difficult to see how a ratio of two statistically-

derived EMs can represent variation in current speed. The origin of the current is not certain as there are three possibilities; the ACC (moving south in warm periods, flowing eastward), a deepening of the Antarctic Slope Current (flowing westward), or resumption of Antarctic Bottom Water production from the emerging shelf during deglaciation (flowing down and along slope to the west). The latter is favoured by the Manganese data of Wu et al. These possibilities certainly allow source changes for sediments arriving at this site.

## 5. Discussion

Our proposed method of discriminating between current-sorted and unsorted fine fractions is applicable to all fine grained deposits, not only the high-latitude cases with coarse IRD treated here. It is straightforward to construct numerous parameter ratios with claimed significance, but if the basic material does not conform to certain standards, then the claimed significance is unsustainable. We suggest that, for the inference of past current vigour based on fine fraction particle size, the correlation between $\overline{SS}$ and SS% provides a standard for acceptance of portions of a record that can be safely interpreted as indicating past flow speed. Our proposal is that running downcore correlation less than 0.5 designate sections of a record whose $\overline{SS}$ values should be rejected as a proxy for current strength.

There is a common supposition that addition of IRD results in coarser $\overline{SS}$ values. Sometimes this is supported by data (e.g. Jonkers et al., 2015). But not all IRD provides sediment with high values of coarse SS (higher % for >25 μm than for 25-10

μm), because in several cases the fine SS fraction (10-25 μm) dominates (Andrews and Principato, 2003) (Supplementary Information #5).

The performance of EMs in distinguishing flow speed in IRD-affected sediment has an uneven performance. The EM ratio of Wu et al. (2018) does not relate at all closely to flow speed at Prydz Bay slope, but it does at Gardar Drift where the EM ratio of Jonkers et al. (2015) does not. Some of the EMs relate closely to SS%. But that is not the key point which is that EMs do not help discriminate good (i.e. sorted) from dubious records. Jonkers et al. proposed that their ratio EM2/EM1 provides a current proxy with no influence of IRD ("*...it is possible to correct for the contribution of IRD and obtain an estimate of changes in bottom current speed by using the ratio of EM2/EM1 ....*"), but in the case of very slow current and abundant IRD input resulting in unsorted fines, it is not clear that this could be a flow speed indicator, but is simply a grainsize indicator free of IRD influence.

In some cases there appears to be a correspondence between high values of the sortable silt mean size and coarse IRD percentage. This could be due to rapid input of IRD which overwhelms the capacity of a current system to resuspend, transport and deposit fine material, resulting in a low correlation between $\overline{SS}$ and SS%. It is also possible that a high flow speed causes reduced deposition rate of the fine fraction leading to an increase in coarse IRD percentage. Very low flow speed leads to lack of sorting in the fine fraction whether or not accompanied by coarse IRD. A high rate of sediment input via ice rafting or meltwater plumes, if accompanied by slow flow or flow where intermittent resuspension events are few

and far between, would lead to an unsorted deposit from which inference of flow speed changes could not be made.

The 63 μm upper limit for the sortable silt calculations was proposed in 1995 partly on the basis that many grain size analyses show a minimum in the very fine sand region, and because that size is conventionally used (by geologists) as the coarse limit of "mud", i.e. silt-clay mixtures. It is certainly the case that under strong currents the size sorting effect continues up into the very fine sand class (63-125 μm), and several datasets demonstrate this (e.g. Lamy et al. (2015) as well as examples from Flemish Pass (Mao et al., 2018). The trouble is that in order to make comparisons a common basis has to be employed and for better or worse the range 10 to 63 μm is now embedded in the literature. The lower limit is close to the cohesive limit of ~8 μm deduced by Mehta and Letter (2013).

The plots of $\overline{SS}$ vs SS% with RMA fits (passing through the respective mean values) are characterised by a slope and an $\overline{SS}$ intercept at SS% = 0. The intercepts decrease with increasing slopes of the plots of $\overline{SS}$ vs SS% as is expected given the fairly narrow range of mean values of the variables (Fig. 7). There is a poor relationship of slopes to flow speed proxies, making it a weak proxy for the efficiency of fine sediment sorting.

The decoupling of fine from coarse IRD under current-controlled systems could be tested via mineralogical and geochemical examination of the coarse and fine fractions which could show differences in provenance. However, the clay fraction is

more likely to be homogenised along a flow path and not show the degree of localisation displayed by coarse glacial inputs (e.g. Andrews et al., 2016; 2018).

The type of analysis presented here requires a measurement of the sortable silt percentage which may be obtained through analyses by Sedigraph and laser particle sizers but not the Coulter counter which provides only $\overline{SS}$. This is unfortunate as the Coulter counter provides excellent size data that has been widely used in recent studies (e.g. Thornalley et al, 2018). A possible way out of this problem is to conduct a 'one shot' pipette analysis at 10 μm on the < 63 μm wet-sieved fine fraction. With a $10^{-4}$ place balance this can be conducted on relatively small samples rather than the usual 20 g (Galehouse, 1971; Folk, 1974).

## 6. Conclusions

Our conclusions are quite straightforward; 1. An inference of current speed based on grain size parameters of fine sediment is only valid if it can be demonstrated that the sediment is actually current-sorted. 2. Sorting in the 'sortable silt' size range (10-63 mm) can be demonstrated through the correlation between the mean size and percentage of sortable silt. 3. For downcore records this can be implemented via the running correlation on a 5- to 9-point basis depending on sampling resolution. 4. The fine fraction of many high latitude sediments under major current systems is demonstrated to be well sorted, affording credible palaeocurrent data despite the presence of significant quantities of coarse IRD. 5. End Member modelling sorts sediments into groups that may have a statistical rather

than genetic basis (associations as in sedimentary facies), and thus does not discriminate groups of data that may not be validly interpreted as representing palaeoflow variations. 6. Correlation between coarse IRD abundance and the silt mean size may reflect either high speed causing reduced fine deposition, or a too high input rate of IRD to a current that is unable to sort the fine fraction (either high rate or slow current or both, especially in glacials).

**Acknowledgements**

We are most grateful to those authors who have provided us with data either on request or via online repositories. Many data sets come from JTA's lab under the careful watch of Wendy Roth to whom thanks are due. This work was not funded by any agency, though acquisition of the data sets was supported by many agencies internationally. We thank Simon Crowhurst for running the Paterson & Heslop (2015) EM decomposition on several records. We are grateful for reviews by David Piper and an anonymous reviewer that helped improve clarity and consideration of transport mechanisms.

## References

Andrews, J.T., 2000. Icebergs and iceberg rafted detritus (IRD) in the North Atlantic: Facts and assumptions. *Oceanography* **13**, 100-108.

Andrews, J.T., 2011. Unravelling sediment transport along glaciated margins (the northwestern Nordic Seas) using quantitative X-ray diffraction of bulk (< 2 mm) sediment, in: Bhuiyan, A.F. (Ed.) *Sediment Transport*, InTech, 225-248.

Andrews, J. T., Bjork, A. A., Eberl, D. D., Jennings, A. E., Verplanck, E. P., 2015. Significant differences in late Quaternary bedrock erosion and transportation: East versus West Greenland ~ 70°N and the evolution of glacial landscapes. *J. Quat. Sci.* 30, 452-463.

Andrews, J.T., Klein, A.J., Jenner, K.A., Jennings, A.E., Campbell, C., 2018. The variability of Baffin Bay seafloor sediment mineralogy: The identification of discrete glacial sediment sources and application to Late Quaternary downcore analysis. *Canadian J. Earth Sci*. 55, 620–639.

Andrews, J. T., Principato, S. M., 2002. Grain-size characteristics and provenance of ice-proximal glacial marine sediments. In: Dowdeswell, J. A. and O'Cofaigh, C. (eds), *Geol. Soc. London, Spec. Publ*. **203**, 305-324.

Andrews, J. T., Stein, R., Moros, M., Perner, K., 2016. Late Quaternary changes in sediment composition on the NE Greenland margin (~73° N) with a focus on the fjords and shelf. *Boreas* **45**, 381–397.

Andrews, J.T., Syvitski, J.P.M., 1994. Sediment fluxes along high latitude continental margins (NE Canada and E. Greenland), in: Hay, W. (Ed.), *Material fluxes on the surface of the Earth*. National Academy Press, Washington, D.C., 99-115.

Andrews, J.T., Voelker, A.H.L., 2018. "Heinrich events" (& sediments): A history of terminology and recommendations for future usage. *Quat. Sci. Rev.* **187**, 31-40.

Andrews, J. T. and Vogt, C., 2014: Source to Sink: Statistical identification of regional variations in the mineralogy of surface sediments in the western Nordic Seas (58°N – 75°N; 10° W -- 40°W). *Mar. Geol*. 357, 151-162.

Barker, S., Chen, J., Gong, X., Jonkers, L., Knorr, G., Thornalley, D., 2015. Icebergs not the trigger for North Atlantic cold events. *Nature* 520, 333-336.

Barnes, P.W., Reimnitz, E., Fox, D., 1982. Ice rafting of fine-grained sediment, a sorting and transport mechanism, Beaufort Sea, Alaska. *J. Sed. Res*. 52, 493-502. doi: 10.1306/212F7F86-2B24-11D7-8648000102C1865D

Blockley, S.P.E. and 9 others, 2012. Synchronisation of palaeoenvironmental records over the last 60,000 years,and an extended INTIMATE event stratigraphy to 48,000 b2k. *Quat. Sci. Rev.* 36, 2-10.

Blott, S.J., Pye, K., 2001. GRADISTAT: A grain size distribution and statistics package for the analysis of unconsolidated sediments: *Earth Surf. Proc. Landforms* 26, 1237-1248.

Chen, F.H., Jia, J., Chen, J.H., Li, G.Q., Zhang, X.J., Xie, H.C., Xia, D.S., Huang, W., An, C.B., 2016. A persistent Holocene wetting trend in arid Central Asia, with wettest conditions in the late Holocene, revealed by multi-proxy analyses of loess-paleosol sequences in Xinjiang. *China Quat. Res*. 146, 134–146.

Darby, D. A., Andrews, J. T., Belt, S. T., Jennings, A. E., and Cabedo-Sanz, P., 2017: Holocene cyclic records of ice-rafted debris and sea ice variations on the East Greenland and Northwest Iceland margins. *Arctic Antarctic and Alpine Research,* 49, 649-672.

deGelleke, L., Hill, P.S., Kienast, M., Piper, D.J.W., 2013. Sediment dynamics during Heinrich event H1 inferred from grain size. *Mar. Geol.* 336, 160-169.

Dethleff, D., Kuhlmann, G., 2009. Entrainment of fine-grained surface deposits into new ice in the southwestern Kara Sea, Siberian Arctic. *Cont. Shelf Res*. 29, 691-701.

Dowdeswell, J.A., Whittington, R.J., Jennings, A.E., Andrews, J.T., Mackensen, A., Marienfeld, P., 2000. An origin for laminated glacimarine sediments through sea-ice build-up and suppressed iceberg rafting. *Sedimentology* 47, 557-576.

Dreimanis, A., 1976. Tills: Their origin and properties, in: Legget, R.F. (Ed.), *Glacial Till an Inter-disciplinary Study. Roy. Soc. Canada Spec Publ.* **12**, 11-49.

Dreimanis, A., 1979. The problems of waterlain tills, in: Schlüchter, C. (Ed.), *Proceedings INQUA Symposium on Genesis and Lithology of Quaternary Deposits Moraines and varves. Origin, genesis, classification*. A.A. Balkema, Rotterdam, 167-177.

Drewry, D., 1986. *Glacial Geologic Processes*. Edward Arnold, London.

Dunhill, G. 2005. *Iceland and Greenland margins: A comparison of depositional processes under differnt glaciological and oceanographic settings*. Ph.D Thesis, Geological Sciences. University of Colorado, Boulder, 258 pp.

Dunhill, G., Andrews, J.T., McCave I.N., Syvitski, J.P.M., in prep. Sedimentation on the Snorri Drift: A ~250 ka record of ice sheet and ocean interactions.

Flemming B.W., 1978. Underwater sand dunes along the southeast African continental margin—observations and implications. *Mar. Geol.* 26, 177-198.

Folk, R.L., 1974, *Petrology of Sedimentary Rocks*. Hemphill Publishing Co., Austin, TX, 182 p.

Folk, R.L., Ward, W.G., 1957. Brazos River bar: A study in the significance of grain size parameters. *J. Sed. Petrol.* 27, 3-26.

Galehouse, J. S. 1971, Sedimentation analysis, Chapter 4, in *Procedures in Sedimentary Petrology*, R. E. Carver (ed.), pp. 69-94, Wiley-Interscience, New York.

Gammon, P.R., Neville, L. A., Patterson, R.T., Savard, M.M., Swindles, GT., 2017. A log-normal spectral analysis of inorganic grain-size distributions from a Canadian boreal lake core: Towards refining depositional process proxy data from high latitude lakes. *Sedimentology* 64, 609-630.

Hoogakker, B., Chapman, M.R., McCave, I.N., Hillaire-Marcel, C., Ellison, C., Hall, I.R., Telford, I. Dynamics of North Atlantic deep water masses during the Holocene. *Paleoceanography* **26**, PA4214, 10 pp., doi:10.1029/2011PA002155

Hudson, B., Overeem, I., McGrath, D., Syvitski, J.P.M., Mikkelsen, A., Hasholt, B., 2014. MODIS observed increase in duration and spatial extent of sediment plumes in Greenland fjord. *Cryosphere* 8, 1161-1176.

Inman, D. L., 1952. Measures for describing the size distribution of sediments. *J. Sed. Petrol.* 22, 125-145.

Jennings, A., Andrews, J., Wilson, L., 2011. Holocene environmental evolution of the SE Greenland shelf north and south of Denmark Strait: Irminger and East Greenland current interactions. *Quat. Sci. Rev*. 30, 980-998.

Jennings, A.E., Andrews, J.T., et al., 2018. Baffin Bay paleoenvironments in the LGM and HS1: Resolving the ice-shelf question. *Mar. Geol.* 402, 5-16.

Jennings, A.E., Andrews, J.T., Oliver, B., Walczak, M., Mix, A. C., 2019. Retreat of the Smith Sound Ice Stream in the early Holocene. *Boreas*, doi: 10.1111/bor.12391

Jia J., Liu, H., Gao, F.Y., Xia, D.S., 2018. Variations in the westerlies in Central Asia since 16 ka recorded by a loess section from the Tien Shan Mountains. *Palaeogeog., Palaeoclim., Palaeoecol.* **504**, 156-161.

Jonkers, L., Barker, S., Hall, I.R., Prins M.A., 2015. Correcting for the influence of ice-rafted detritus on grain size-based paleocurrent speed estimates. *Paleoceanography* **30**, 1347–1357,

Kleiven, H.F., Hall, I.R., McCave, I.N., Knorr, G., Jansen, E., 2011. Coupled deep-water flow and climate variability in the Mid-Pleistocene North Atlantic. *Geology* **39**, 343-346.

Konert, M., Vandenberghe, J., 1997, Comparison of laser grain size analysis with pipette and sieve analysis: A solution for the underestimation of the clay fraction. *Sedimentology* 44, p. 523-535.

Lamy, F., Arz, H.W., Kilian, R., Lange, C.B., Lembke-Jene, L., Wengler, M., Kaiser, J., Baeza-Urrea, O., Hall, I.R., Harada, N., Tiedemann, R., 2015. Glacial reduction and millennial-scale variations in Drake Passage throughflow. *Proc. Natl. Acad. Sci. U.S.A.* **112**, 13496–13501. doi:10.1073/pnas.1509203112

Li, G., Piper, D.J.W., 2015. The influence of meltwater on the Labrador Current in Heinrich Event 1 and the Younger Dryas. *Quat. Sci. Rev.* **107**, 129-137

Lisiecki, L.E., Raymo, M.E., 2005. A Pliocene-Pleistocene stack of 57 globally distributed benthic $\delta^{18}O$ records. *Paleoceanography* 20, 17pp., PA1003, doi: 10.1029.2004PA001071.

Mao, L., Piper, D.J.W., Saint-Ange, F., Andrews, J.T., 2018. Labrador Current fluctuation during the last glacial cycle. *Mar. Geol.* **395**, 234-246.

Marshall, N.R., Piper, D.J.W., Saint-Ange F., Campbell, D.C. 2014. Late Quaternary history of contourite drifts and. variations in Labrador Current flow, Flemish Pass, offshore eastern Canada. *Geo-Mar. Lett.* **34**, 457–470, doi: 10.1007/s00367-014-0377-z

McCave, I.N., Andrews, J.T., in prep Distinguishing current effects in sediments delivered to the ocean by ice. II. Glacial to Holocene changes in high latitude North Atlantic flows. *Quat. Sci. Rev.,* .

McCave, I.N., Manighetti, B., Robinson, S.G., 1995a. Sortable silt and fine sediment size/ composition slicing: parameters for palaeocurrent speed and palaeoceanography. *Paleoceanography* **10**, 593-610.

McCave I.N., Hall, I.R., 2006. Size sorting in marine muds: Processes, pitfalls and prospects for palaeoflow-speed proxies. *Geochem. Geophys. Geosyst.* **7**, Q10N05, 37 pp. doi: 10.1029/2006GC001284.

McCave, I.N., Hall, I.R., Bianchi, G.G., 2006. Laser vs. settling velocity differences in silt grainsize measurements: estimation of palaeocurrent vigour. *Sedimentology* **53**, 919-928.

McCave, I.N., Thornalley, D.J.R., Hall, I.R., 2017. Relation of sortable silt grain size to deep-sea current speeds: Calibration of the 'Mud Current Meter' *Deep-Sea Res. Part I* **127**, 1-12.

McIntyre K.L., Howe, J.A., 2009. Bottom-current variability during the last glacial-deglacial transition, Northern Rockall Trough and Faroe Bank Channel, NE Atlantic. *Scottish J. Geol.* **45**, 43-57.

McKay, R., Golledge, N.R., Maas, S., Naish, T., Levy, R., Dunbar, G., Kuhn, G., 2016. Antarctic marine ice-sheet retreat in the Ross Sea during the early Holocene. *Geology,* **44**, 7-10.

Mehta, A.J., Letter, J.V., 2013. Comments on the transition between cohesive and cohesionless sediment bed exchange. *Estuar., Coast. Shelf Sci*. **131**, 319–324.

Miller, R.L. and Kahn, J.S., 1962. *Statistical analysis in the geological sciences*. Wiley, New York, 483 pp

Miller, M.C., McCave, I.N., Komar, P.D., 1977. Threshold of sediment motion under unidirectional currents. *Sedimentology* **24**, 507-527.

Niño, Y., Lopez, F., Garcia, M., 2003. Threshold for particle entrainment into suspension. *Sedimentology* 50, 247-263.

Nürnberg, D., Wollenburg, I., Dethleff, D., Eicken, H., Kassens, H., Letzig, T., Reimnitz, E., Thiede J., 1994. Sediments in Arctic sea ice—entrainment, transport and release. *Mar. Geol.* 119, 185–214.

Paterson, G. A., Heslop, D., 2015. New methods for unmixing sediment grain size data, *Geochem. Geophys. Geosyst*. **16**, 4494–4506, doi:10.1002/ 2015GC006070.

Reeh, N., 2004. Holocene climate and fjord glaciations in Northeast Greenland: implications for IRD deposition in the North Atlantic. *Sed. Geol.* 165, 333-342.

Reeh, N., Mayer, C., Miller, H., Thomsen, H.H., Weidick, A., 1999. Present and past climate control on fjord glaciations in Greenland: Implications for IRD-deposition in the sea. *Geophys. Res. Lett.* 26, 1039-1042.

Seidel, M., Hlawitschka, M., 2015. An R-based function for modeling of end member compositions. *Math. Geosci*. **47**, 995–1007. doi: 10.1007/s11004-015-9609-7

Stein, R., 2008. *Arctic Ocean Sediments. Processes, Proxies, and Paleoenvironment.* Elsevier, New York.

Syvitski, J.P.M., 1988. On the deposition of sediment within glacier-influenced fjords: Oceanographic controls. *Mar. Geol.* **85**, 301-329.

Syvitski, J.P.M., Andrews, J.T., Dowdeswell, J.A., 1996. Sediment deposition in an iceberg-dominated glacimarine environment, East Greenland: Basin fill implications. *Global Planet. Change* **12**, 251-270.

Thornalley, D.J.R. and 12 others, 2018. Anomalously weak Labrador Sea convection and Atlantic overturning during the past 150 years. *Nature* **556** 227-230.

Verplanck, E.P., Farmer, G.L., Andrews, J., Dunhill, G., Millo, C., 2009. Provenance of Quaternary glacial and glacimarine sediments along the southeast Greenland margin. *Earth Planet. Sci. Lett.* **286**, 52-62.

Wanner, H., Solomina, O., Grosjean, M., Ritz, S.P., Jetel, M., 2011. Structure and origin of Holocene cold events. *Quat. Sci. Rev*. **30**, 3109–3123

Weltje, G. J. (1997) End-member modeling of compositional data: Numerical-statistical algorithms for solving the explicit mixing problem, *Math. Geol*., **29**, 503–549. doi: 10.1007/BF02775085.

Wu, L., Wang, R., Xiao, W., Krijgsman, W., Li, Q., Ge, S., Ma, T., 2018. Late Quaternary deep stratification-climate coupling in the Southern Ocean: Implications for changes in abyssal carbon storage. *Geochem., Geophys., Geosyst.*, **19**, 379–395, doi: 10.1002/2017GC007250

Xu, K.H., Bentley, S.J., Robichaux, P., Sha, X.Y. & Yang, H.F., 2016. Implications of texture and erodibility for sediment retention in receiving basins of coastal Louisiana Diversions. *Water* **8**, Art. No. 26, doi: 10.3390/w8010026

# Figures

**Fig. 1**. Cartoon of two settings for deposition of ice-rafted and plume-delivered sediment: A) Sediment falls out into a fast current, fines are removed to downstream locations where they are deposited at a place where the current is slower forming a drift, while coarse material falls directly to the bed at the point of release where it remains. B) Sediment falls out into a slow current and all material falls directly to the bed close to the point of release.

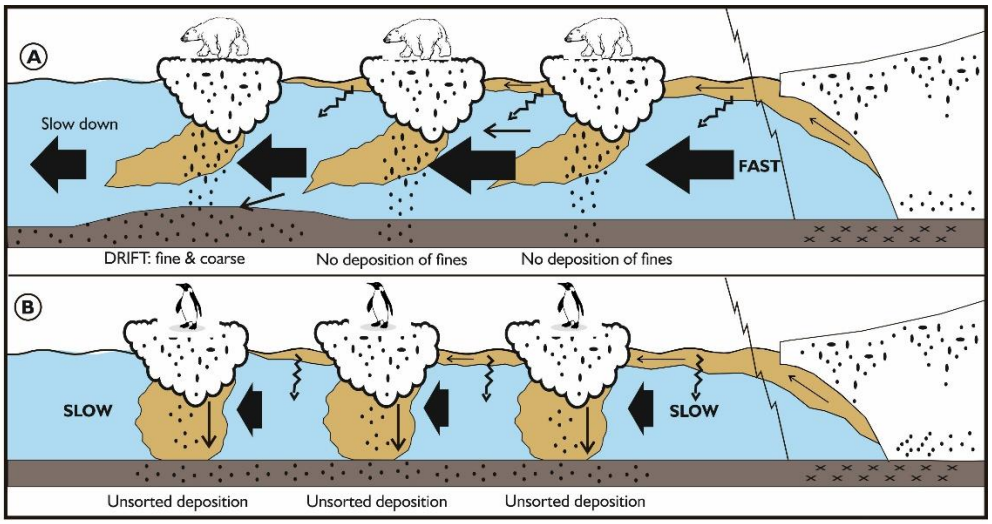


**Fig. 2**. Sediments from Baffin Bay, west Greenland (Cruise HU200037): A) Well sorted surface sediments; B) Poor relationship between $\overline{SS}$ and coarse IRD (%>240 µm).

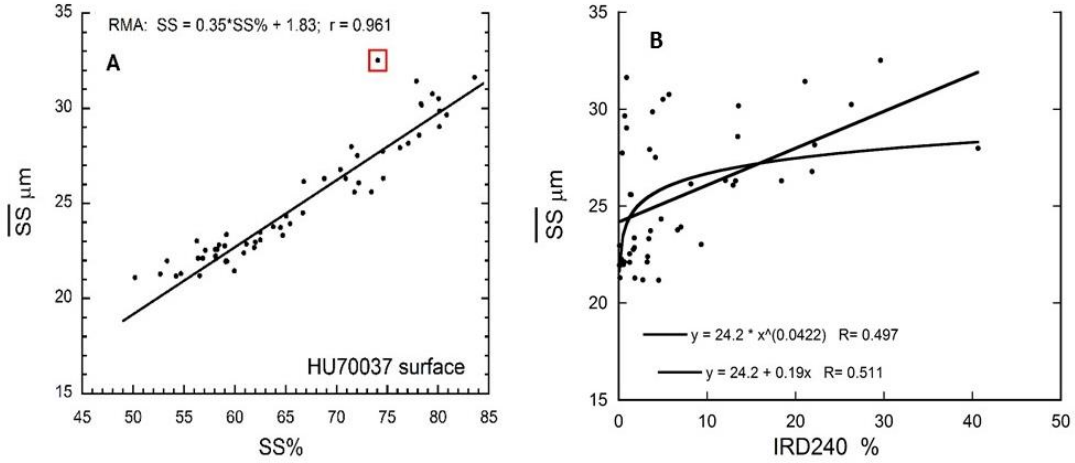

**Fig. 3**. Data from diamicts in marine cores: A) $\overline{SS}$ vs SS% showing no significant sorting relationship, B) $\overline{SS}$ vs % IRD>240 μm showing a weak negative relationship (i.e. more IRD associates with finer sortable silt). Red boxed points omitted from correlations.

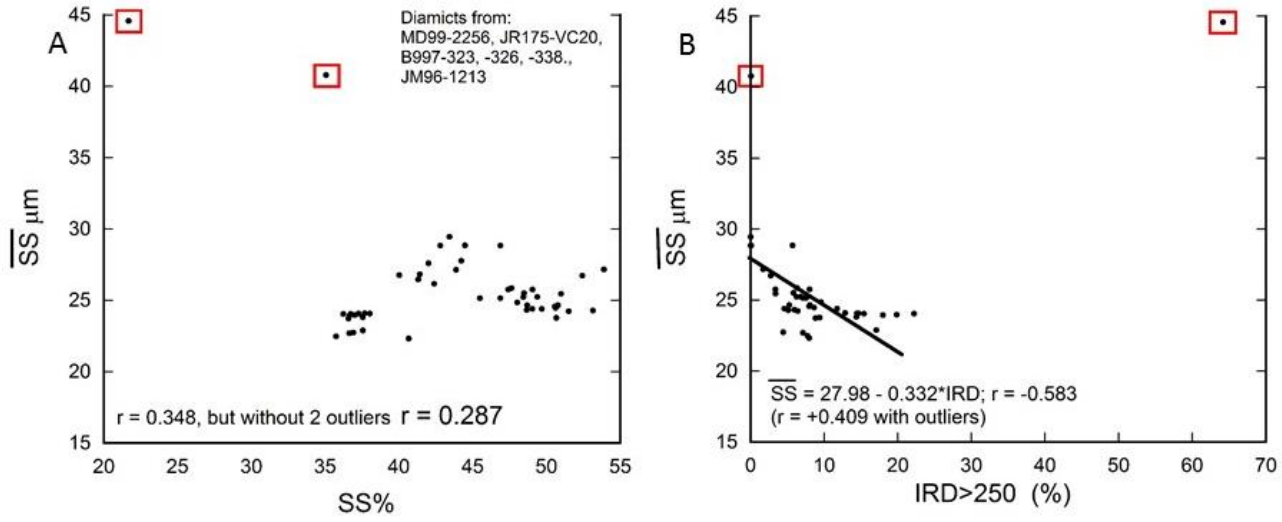


**Fig. 4**. Data from A) Mississippi delta top basins (Xu et al., 2016) showing no significant relationship between $\overline{SS}$ and SS%, and B) from 'Lake E' (Gammon et al., 2017) where two unsorted clusters are apparent plus a well sorted tail of material with SS% > 62.5% which occupies two discrete sections of the core.

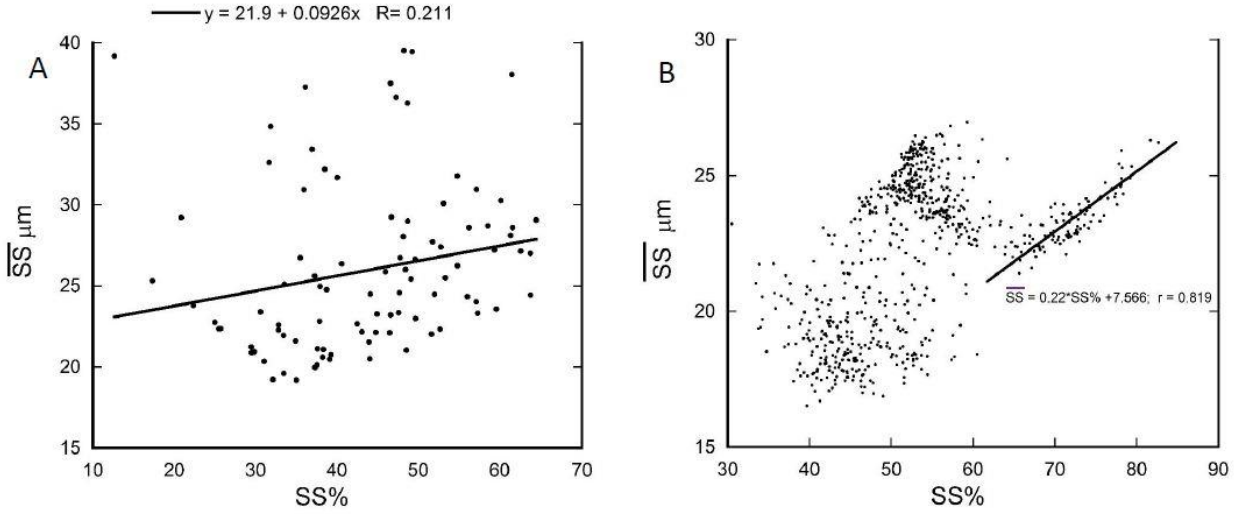

**Fig. 5**. Example of running downcore correlations with varying window size for MD99-2323 with 5, 7, 9 and 13 point correlations. The horizontal lines are set at r = 0.5. The scale for 7 and 13 point is offset but has the same absolute range. Red (7pt) or blue (9pt ) are preferred. Where the number of data points is low the 7-point correlation may be preferable.

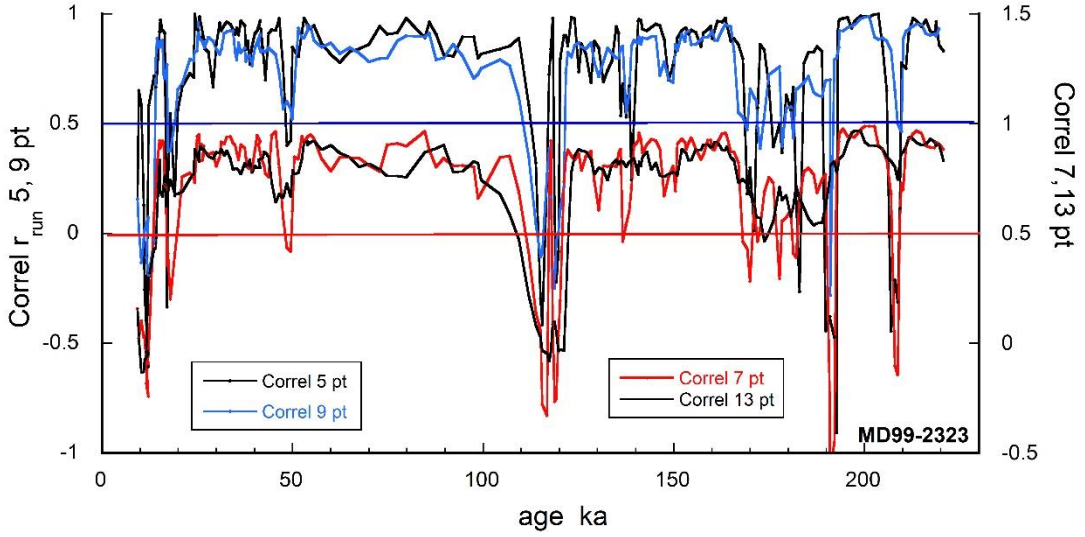


**Fig. 6**. $\overline{SS}$ and IRD250% with 9-point correlation ($r_{run}$), for MD99-2323. The blue highlights here mark sections where the 9-point correlation coefficient $r_{run}$ is below 0.5, for which the validity of the sortable silt record would be in doubt. There is no obvious correspondance between $r_{run}$ and coarse IRD250 % save at 118-123 ka and the top of the core age <14 ka. The yellow bars marks a piece with $r_{run}$ around 0.5.

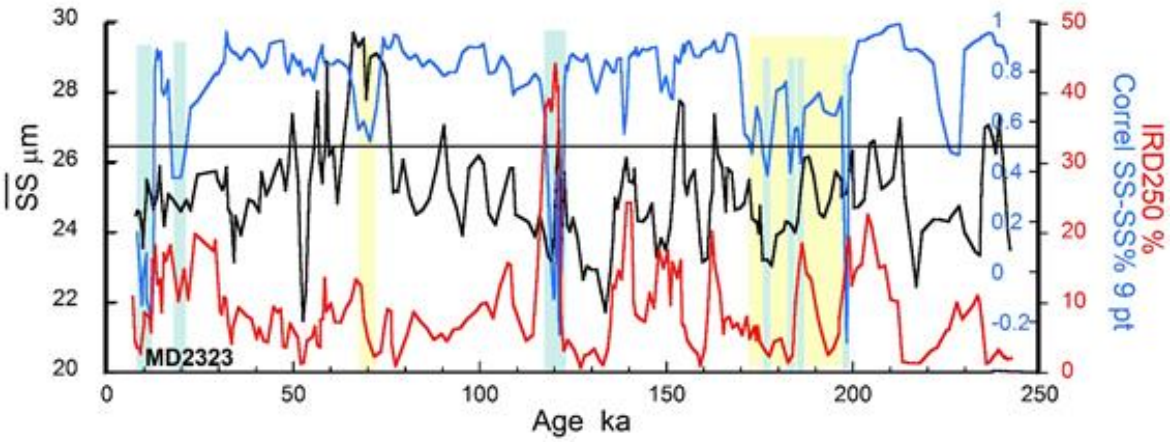

**Fig. 7**. **A**. Plot of slope versus intercept on the SS% = 0 axis for 41 downcore records of $\overline{SS}$ vs SS%. Possibly steeper slopes above 0.35 indicate higher efficiency of sorting. All the records are well sorted as indicated by $r_{run}$ >0.7. **B**. Histogram of whole record r values (see Table 2) with most > 0.80. **C.** Histogram of all $r_{run}$ values from the marine cores listed in Table 2. These are for groups of 9 or 7 points. Dashed line marks the cut-off for acceptability ($r_{run}$ < 0.5). More than 50% of the values are r > 0.8 and 79% are r > 0.5.

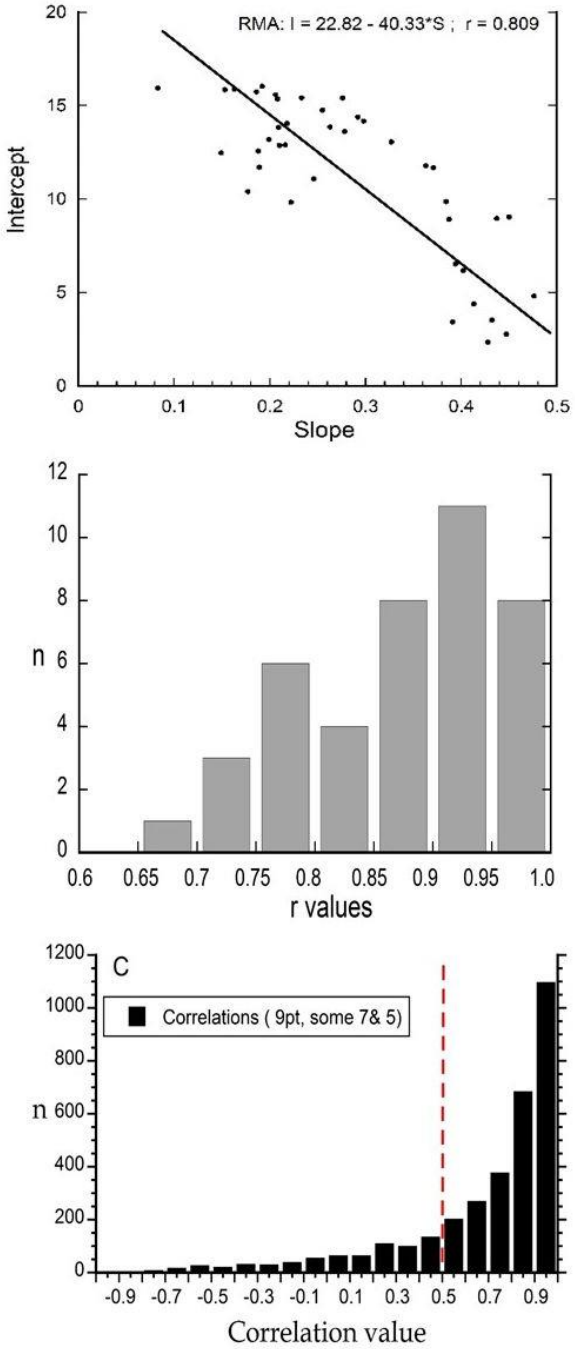

**Fig. 8.** Examples of 9-point correlation vs $\overline{SS}$-SS% slope where (A) most data are acceptable (r > 0.5; slope > 0.07), and (B) a significant amount of the data record absence of sorting. Yellow areas mark acceptable regions of $r_{run}$ > 0.5 and slope > 0.07.

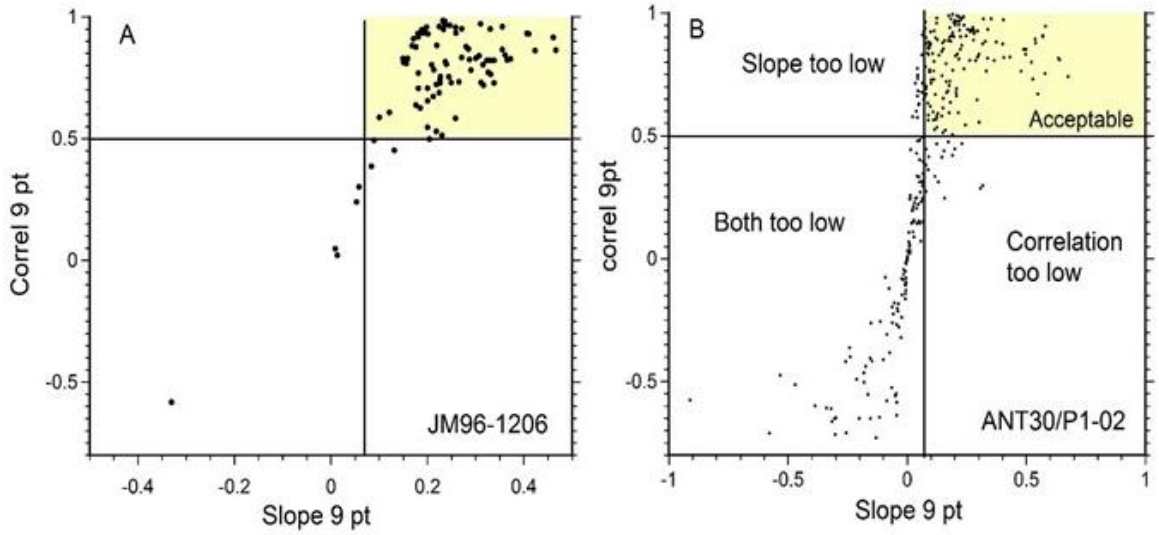


**Fig. 9.** Holocene records of $\overline{SS}$ and IRD250% for East Greenland cores JM 96-1210 and JM 96-1206, and Northwest Iceland core MD 99-2269. The red arrow in the latter record marks the slowdown in flow associated with the 8.2 ka event, and blue pointers mark the 4.2 eventand onset of the 3.2-2.7 event.. Blue bars indicate portions of the records with $\overline{SS}$ - SS% correlation coefficients below 0.5. The inset shows the $\overline{SS}$ vs SS% for core MD2269 where two well sorted groups occur separated at 9.2 ka (dashed line on age plot), suggesting a switch in the size distribution of material supplied to the site, possibly a source change.

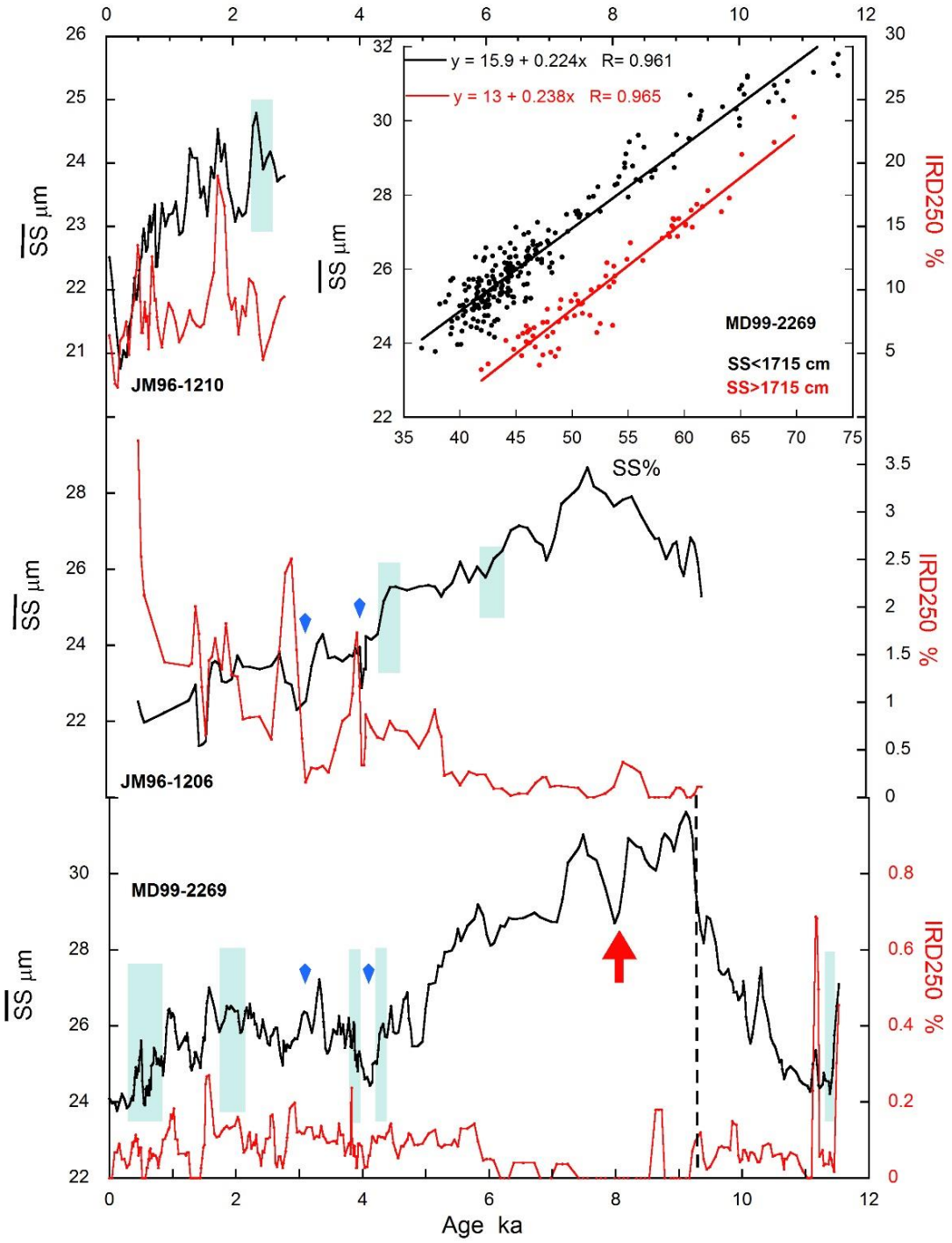
y = 15.9 + 0.224x R= 0.961
y = 13 + 0.238x R= 0.965
MD99-2269
SS<1715 cm
SS>1715 cm
SS µm
SS%
IRD250 %
JM96-1210
JM96-1206
MD99-2269
Age ka

**Fig. 10.** A. $\overline{SS}$ vs SS%, and B. $\overline{SS}$ vs IRD257 for core GC083 from Faroe Bank Channel (McIntyre & Howe, 2009). Only above ~50% IRD does there appear to be an effect of the amount of IRD on $\overline{SS}$ size.

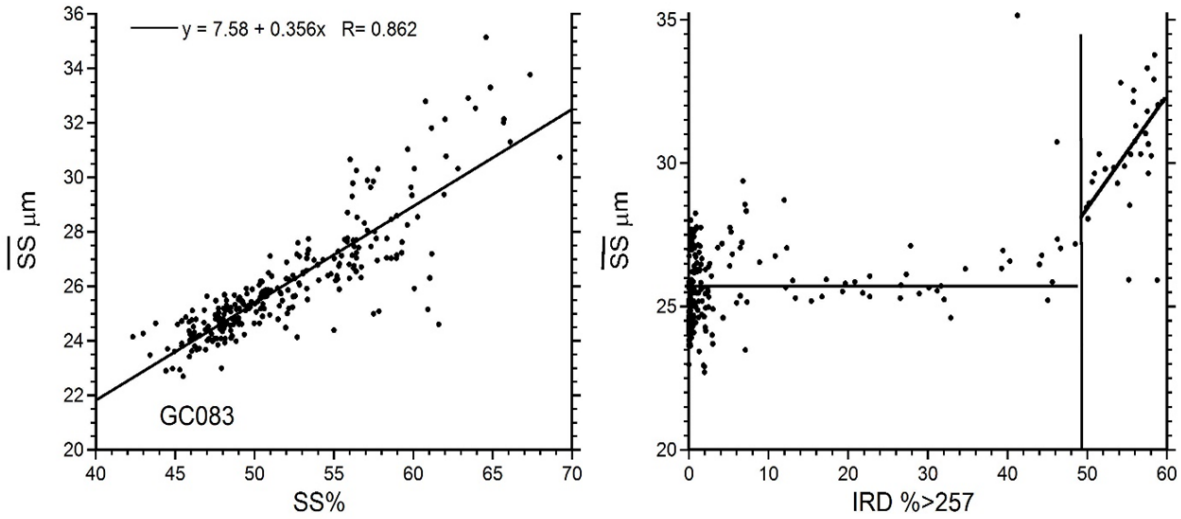


**Fig. 11.** Downcore data from Faroe Bank Channel (FBC) (GC083). The running 9-point correlation (red) lies above 0.7 for much of the record and drops below 0.5 (blue bars) in the Holocene and four periods in MIS 3, three of which do not correspond to high IRD. The Holocene section is mostly unreliable as a flow speed record. The age model is of low resolution, being based on only two C-14 dates and correlation to a nearby core (McIntyre and Howe, 2009).

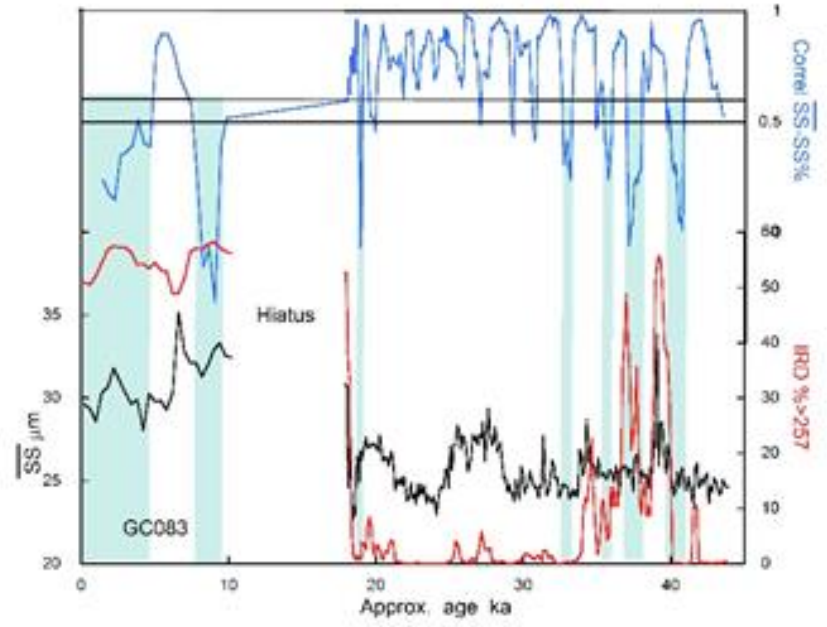

**Fig. 12.** Sortable silt mean size, smoothed IRD150 % and the 7-point correlation for the data of Jonkers et al. (2015) for ODP 983 plotted on the age model of Barker et al. (2015). Blue bars mark periods with $r_{run} < 0.5$. Note slow flow in the LGM and Heinrich-1 (GS-2 in the INTIMATE stratigraphy of Blockley et al., 2012) (23 to 16 ka), and variable influence of coarse IRD on fine sorting (e.g. strong at 34-35, 30.5-31.5, and 12.5-13.5 ka but weak at 23-25 and 14-18 ka. (YD = Younger Dryas, H-1 = Heinrich Event-1, H-2, -3 = Heinrich layers 2 & 3, the IRD peak at 34-35 ka is probably GS-7).

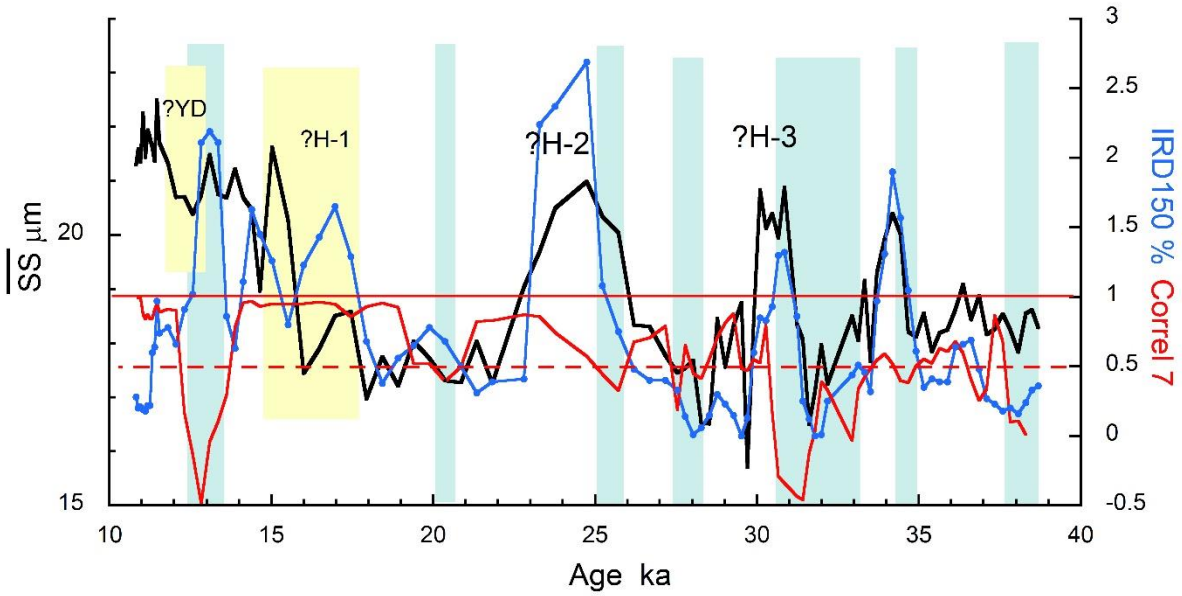


**Fig. 13. A.** End Member decomposition of the size distributions at ODP 983 from 39 to 11 ka (see Fig. 12). EM-1 is suggested to represent an IRD contribution by Jonkers et al. (2015, see panel B for their EMs) but it also correlates at r = 0.956 with SS%, although EM-3 also contains material into the medium sand range of IRD origin. **C.** Relationship of EM ratios to the sortable silt mean size. The ratio EM2/EM1 proposed as a flow speed indicator by Jonkers et al. (2015) shows no relation to $\overline{SS}$ whereas the ratio EM2/(EM2 + EM1) proposed by Wu et al. (2018) shows an excellent correlation with $\overline{SS}$. **D.** EM3 is almost perfectly correlated with SS%

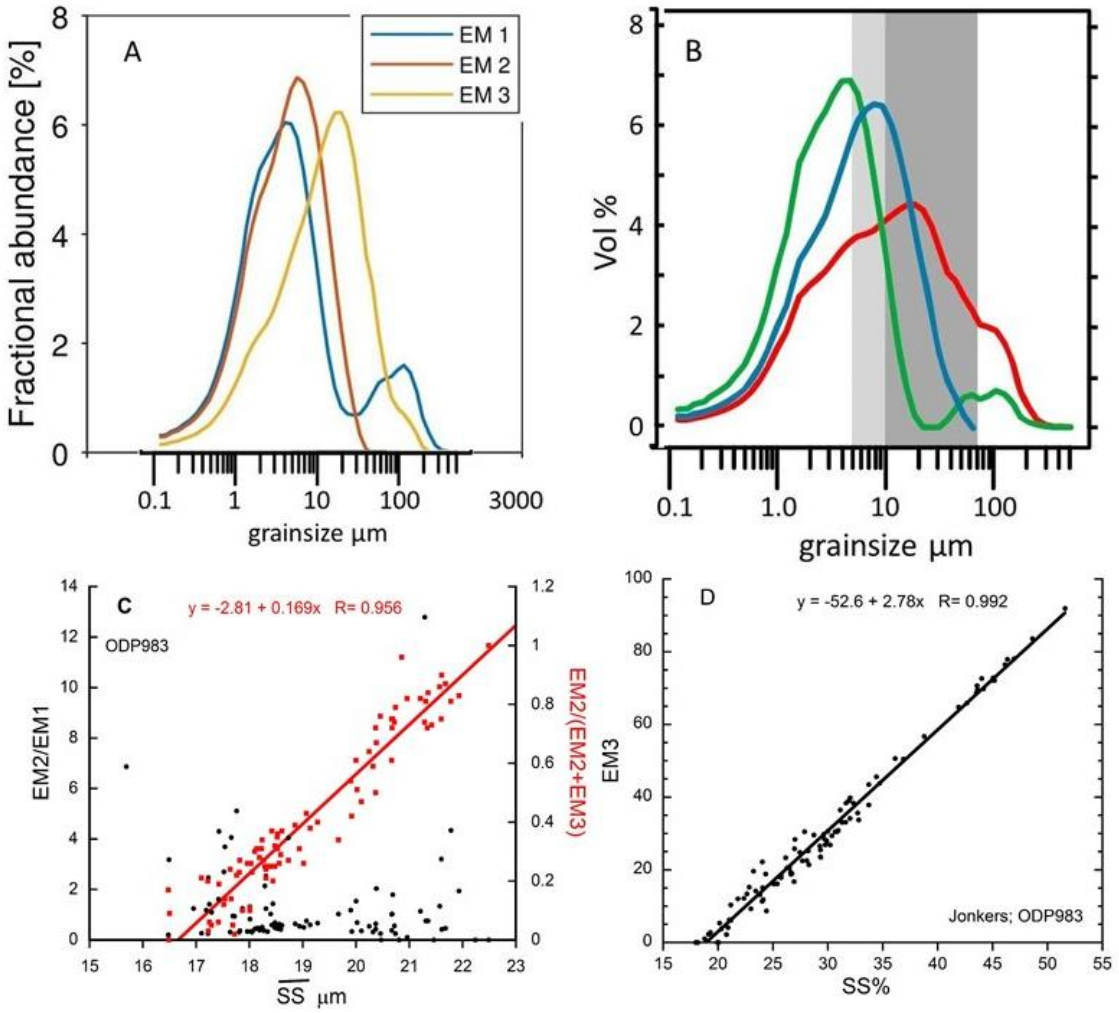


**Fig. 14**. Prydz Bay slope; ANT30/PC1-02. **A**. $\overline{SS}$ vs SS% for $r_{run} > 0.9$ showing two groups separated at SS% ~25. **B**. Two well sorted groups of data from terminations.

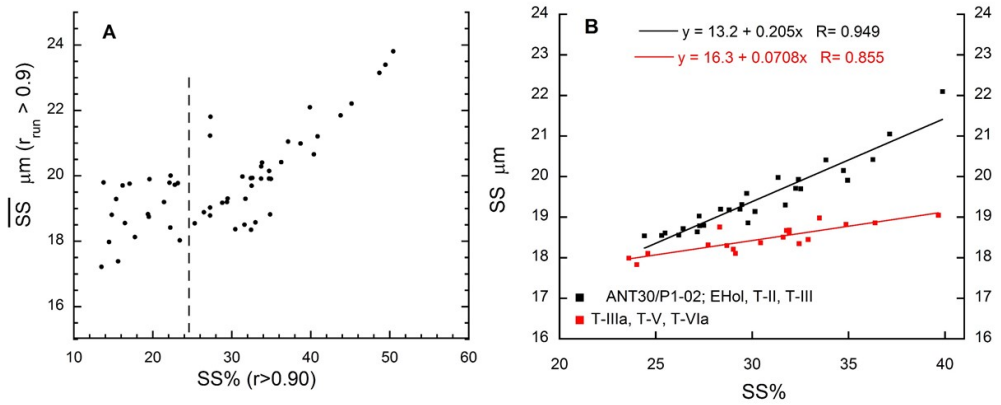

**Fig. 15.** The record of $\overline{SS}$ (3-point averaged) and a 9-point $r_{run}$ with the LR04 $\delta^{18}O$ stack vs age for ANT30/PC1-02. Portions of the record with $r_{run} < 0.5$ are marked in blue (horizontal lines at 0.5 and 0.7), and high correlations in Terminations and sharp cold to warm transitions are marked by purple arrows. As the record is low resolution, average $\Delta t$ is 1.7 ka, the 9-point window is 15 ka, but a similar result is obtained from a 5-point window, 8.5 ka wide (see supplementary Information #6).

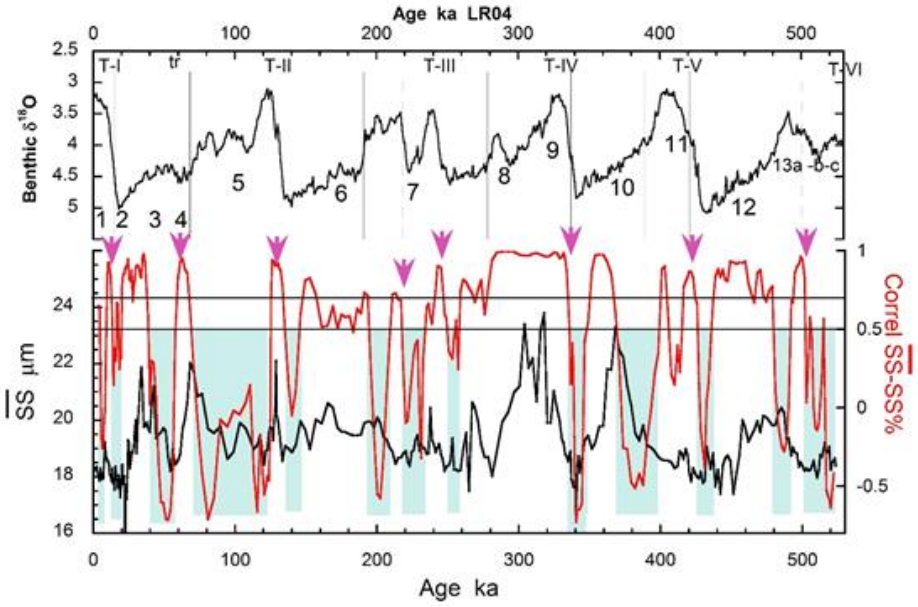


**Fig. 16.** ANT30/P1/02: Relationship of End Members (A) to SS variables. The ratio EM2/(EM1+EM2) proposed by Wu et al. (2018) as a flow speed indicator is almost perfectly correlated with SS% (B), but weakly with $\overline{SS}$ (C).

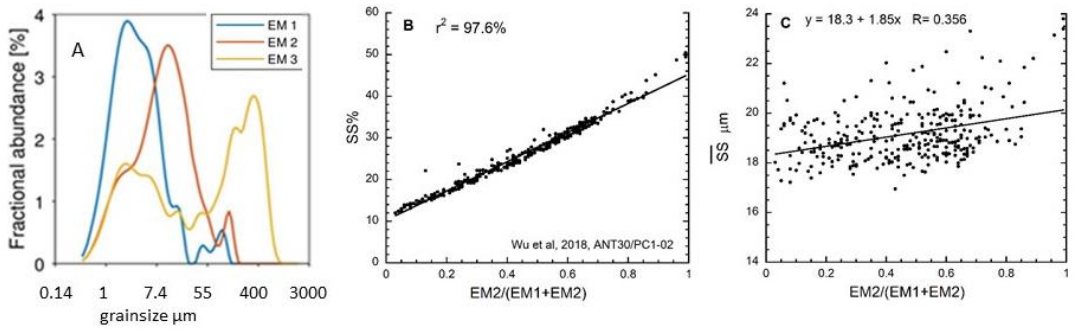

**Table 1**. Core locations. (For references 1-31 see Supplementary Information #10)

| Core # | bott, cm | MIS | location | lat. (N) | long (W) | water depth | Ref # (Supp. Inf |
|---|---|---|---|---|---|---|---|
| **E Greenland/N. Iceland** | | | | | | | |
| JM96-1206 | 288 | 1 | E. Greenland (Nansen Fjd) | 68° 06.0′ | 29° 25.5′ | 405 | 1 |
| JM96-1210 | 330 | 1 | E. Greenland (Nansen Fjd) | 68° 12.0' | 29° 36.0' | 452 | 2, 3 |
| JM96-1213 | 540 | 1 | Kangerlussuaq Trough | 67° 17.3' | 30° 57.6' | 557 | 4 |
| JM96-1215 | 587 | 1 | Kangerlussuaq Trough | 67° 02.8′ | 30° 51.6′ | 668 | 5 |
| JM96-1216 | 250 | 1 | Kangerlussuaq Trough | 65° 57.77′ | 30° 38.0′ | 478 | 6 |
| JM96-1222 | 456 | 2 & 3 | Denmark Str outlet/Snorri | 65° 24.96' | 28° 24.96' | 1045 | 7, 8 |
| JM96-1226 | 255 | 1 | Denmark Str outlet/Snorri | 65° 11.82' | 29° 00.00' | 1519 | 9 |
| JM96-1229 | 255 | 2 & 3 | D'mark Str entr/Blosseville B | 67° 01.02' | 25° 09.00' | 1047 | 9 |
| MD99-2323 | 721 | 2 & 7 | Denmark Str outlet/Snorri | 65° 24.96' | 28° 19.86 | 1062 | 8 |
| MD99-2256 | 1751 | 1 | SW Iceland shelf, Jokuldjup Tr. | 64° 18.19' | 24° 12.40' | 246 | 10, 11 |
| MD99-2260 | 2736 | 1,2,3 | KTMF/?Snorri Drift | 65° 01.2' | 30° 15.0' | 1865 | 8 |
| MD99-2269 | 2494 | 1 | Húnaflóaáll/ NW Iceland | 66° 37.53' | 20° 51.16' | 365 | 12, 13 |
| MD99-2274 | 625 | 1,2,3 | N Iceland slope | 67° 34.95' | 17° 04.41' | 1000 | 14 |
| **Baffin Bay /Nares** | | | | | | | |
| HU2013029-64PC | 702 | | Baffin Island slope | 71° 25.57' | 72° 46,16' | 875 | 15 |
| HU2013029-77PC | 642 | 1,2,3 | Baffin Island slope | 68° 18.53' | 63° 47.68' | 1153 | 16 |
| STL 063 | 421 | | Nares Strait | | | | unpub |
| JR175-VC 05 | 581 | | W Greenland - Baffin Bay | 69° 09.6' | 51° 31.63' | 389 | unpub |
| JR175-VC 09 | 581 | | W Greenland - Baffin Bay | 69° 05.79' | 51° 23.65' | 294 | unpub |
| JR175-VC 20 | 525 | 1 | W Greenland - Baffin Bay | 68° 12.06' | 57° 45.38' | 434 | 17 |
| JR175-VC 24 | 552 | | W Greenland - Baffin Bay | 68° 26.88' | 55° 15.16' | 432 | unpub |
| JR175-VC 32 | 232 | | W Greenland - Baffin Bay | 68° 09.96' | 59° 37.43' | 690 | unpub |
| **Labrador Current/ Flemish Pass** | | | | | | | |
| Hu2006040-40 | 1010 | 1 | N. Labrador Shelf | 58°75.84' | 61°86.87' | 203 | 18 |
| HU2011031-21 | 856 | 1 | Flemish Pass | 46° 45.06' | 46° 41.04' | 991 | 19 |
| Pz96018-006 pc&twc | 155/80 | 1, 2 | Flemish Pass | 47° 44.73′ | 46° 12.19′ | 1050 | 20 |
| Pz96018-008 pc&twc | 120/80 | 1, 2 | Flemish Pass | 47° 37.5′ | 46° 39.08′ | 1050 | 20 |
| Hu2011-59 | 1065 | | Flemish Pass | 48° 43.66′ | 45° 31.17′ | 750 | 21 |
| Hu2011-62 | 1030 | | Flemish Pass | 48° 46.37′ | 45° 27.98′ | 1163 | 21 |
| **Iceland-Scotland Overflows** | | | | | | | |
| GC082 | 247 | | N. Rockall Trough | 59° 43.27' | 07° 10.17' | 1093 | 23 |
| GC083 | 262 | | Faroe Bank Channel | 60° 10.00' | 06° 09.91' | 1226 | 23 |
| ODP 983 | | 1-3, 18-22 | N. Gardar Drift | 60° 24.21' | 23° 03.44' | 1983 | 23, 24 |
| **Other locations** | | | | | | | |
| HLY0501-05JPC | 1701 | 1 | Chukchi Slope | 72° 51.618' | 158° 25.260' | 415 | 25 |
| AMD0214-02PC | 499 | 1 | Beaufort Slope | 71° 22.910' | 133° 34.040' | 998 | 25 |
| MR806-PC09 | 303 | 1 , 2 | N.Drake Passage | **55° 42.58′ S** | 66° 08.06′ | 684 | 26 |
| ANT30/PC-01 | 623 | 1-3 | Prydz Bay Slope | **65° 0.60' S** | **72° 56.4' E** | 2916 | 27 |
| **Other data** | | | | | | | |
| HU70037 | | | W Greenland surface | many | many | many | 28 |
| LJW10 | | | Lujiaowan, Tien Shan, loess | 43° 58.483' | 85° 20.166'' E | +1462 | 29 |
| Miss Delta West Bay | | | Miss Delta West Bay | 29° 7.5' to 10.2' | 89° 17.8' to 19.9' | 1.26 | 30 |
| Miss Delta Big Mar | | | Miss Delta Big Mar | 29° 49.5' to 50.6' | 89° 54.1' to 54.98' | 0.23 | 30 |
| Alberta Lake E | | | Alberta Lake E | 56° 47.60' | 110° 40.68' | 3.75 | 31 |

**Table 2**. Slope and intercept data for $\overline{SS}$ vs SS% downcore data.

**Slopes and intercepts for SSmean on SS% linear regression or RMA**

| core/sample set | Condition | SS% avg | SS avg | slope | intercept µm | r | n | current | instrument |
|---|---|---|---|---|---|---|---|---|---|
| **E Greenland/N. Iceland** | | | | | | | | | |
| JM96-1206 | RMA, all | 46.85 | 24.94 | 0.208 | 15.36 | 0.923 | 93 | EGC | Malvern 2000 |
| JM96-1210 | RMA, all | 30.70 | 23.06 | 0.371 | 11.68 | 0.805 | 66 | EGC | Malvern |
| JM96-1213 | RMA, minus till | 32.59 | 22.30 | 0.192 | 16.04 | 0.783 | 29 | | Malvern |
| JM96-1215 | RMA, all | 46.33 | 23.19 | 0.203 | 13.78 | 0.957 | 117 | | Malvern |
| JM96-1216 | RMA, all | 48.60 | 26.64 | 0.263 | 13.86 | 0.966 | 29 | | Malvern |
| JM96-1222 | | 41.92 | 25.17 | 0.250 | 14.70 | 0.603 | 50 | DNBC | Malvern |
| JM96-1226 | lin regr | | | 0.120 | 18.90 | 0.497 | 24 | DNBC/DS outlet | Malvern |
| JM96-1229 | RMA all | 52.78 | 28.25 | 0.255 | 14.77 | 0.900 | 24 | DS inlet/DSOW | Malvern |
| MD99-2323 | RMA all | 46.68 | 25.11 | 0.210 | 15.29 | 0.722 | 226 | DNBC | Malvern |
| MD2323 + JM1222 | RMA all | 45.80 | 25.23 | 0.207 | 15.75 | 0.720 | 230 | DNBC | Malvern |
| MD99-2260 | RMA all | 52.82 | 29.80 | 0.276 | 15.42 | 0.936 | 108 | DNBC | Malvern |
| MD99-2269 | group <1706 cm | 47.30 | 26.50 | 0.233 | 15.42 | 0.961 | 232 | NIC | Malvern |
| MD99-2269 | group >1706 cm | 52.60 | 25.53 | 0.246 | 11.08 | 0.965 | 74 | NIC | Malvern |
| MD99-2274 | RMA all | 41.87 | 22.59 | 0.209 | 13.84 | 0.773 | 30 | | Malvern |
| **Baffin Bay /Nares** | | | | | | | | | |
| HU2013029- 064PC | RMA | 36.82 | 23.85 | 0.278 | 13.62 | 0.878 | 34 | Baff slope Curr | Malvern |
| HU2013029- 077PC | RMA Correl >0.7 | 31.90 | 22.11 | 0.384 | 9.87 | 0.867 | 43 | Baff slope Curr | Malvern |
| Nares 163 STL | RMA Gp 2 | 43.52 | 22.02 | 0.210 | 12.89 | 0.920 | 24 | Nares Str | Malvern |
| Nares 163 STL | RMA Gp1 | 32.89 | 23.74 | 0.363 | 11.78 | 0.953 | 15 | Nares Str | Malvern |
| | | | | | | | | | Coulter |
| JR175 VC05 | RMA all | 28.59 | 21.91 | 0.450 | 9.06 | 0.944 | 48 | WGC | LS13320 |
| JR175 VC09 | RMA all | 29.83 | 21.99 | 0.437 | 8.96 | 0.951 | 61 | WGC | Coulter |
| JR175 VC20 | RMA all | 44.28 | 25.23 | 0.343 | 10.05 | 0.671 | 39 | WGC | Coulter |
| JR175 VC24 | RMA correl>0.76 | 23.67 | 20.81 | 0.327 | 13.06 | 0.815 | 43 | WGC | Coulter |
| JR175 VC32 | RMA correl>0.77 | 40.46 | 26.22 | 0.298 | 14.18 | 0.811 | 16 | WGC | Coulter |
| **Labrador Current/Flemish Pass** | | | | | | | | | |
| Hu2006040-40 | RMA all PC & TC | 53.90 | 24.65 | 0.163 | 15.890 | 0.911 | 207 | LC | Coulter |
| HU2011031-21 TC | RMA all TC | 56.34 | 26.44 | 0.428 | 2.34 | 0.901 | 38 | LC | Coulter |
| HU2011031-21 PC | RMA all PC | 50.87 | 26.55 | 0.394 | 6.53 | 0.880 | 30 | LC | Coulter |
| HU2011031-21 PC+TC | RMA all PC+TC | 53.93 | 26.49 | 0.387 | 5.63 | 0.841 | 68 | LC | Coulter |
| Li&P 96-6 PC | RMA all PC | 52.95 | 25.56 | 0.218 | 14.04 | 0.709 | 68 | LC | Coulter |
| Li&P 96-6 TC | RMA all TC | 57.51 | 25.93 | 0.391 | 3.43 | 0.709 | 38 | LC | Coulter |
| Li&P 96-8 PC& TC | RMA all PC & TC | 55.49 | 27.51 | 0.432 | 3.53 | 0.946 | 75 | LC | Coulter |
| HU2011031-59PC | RMA all | 48.64 | 24.79 | 0.186 | 15.74 | 0.812 | 214 | LC | Malvern |
| HU2011031-62PC | RMA all | 38.04 | 25.50 | 0.292 | 14.39 | 0.689 | 207 | LC | Malvern |
| **Iceland-Scotland Overflows** | | | | | | | | | |
| GC082 | RMA, all | 49.44 | 26.05 | 0.402 | 6.16 | 0.973 | 241 | ISOW | Coulter |
| GC083 | RMA, all | 51.99 | 26.10 | 0.413 | 4.39 | 0.862 | 262 | ISOW | Coulter |
| ODP 983 MIS 2 -3 | RMA all | 29.83 | 19.12 | 0.199 | 13.19 | 0.776 | 95 | ISOW | Fritsch |
| ODP983, MIS 18-22 | RMA all | 26.99 | 16.81 | 0.189 | 11.70 | 0.898 | 439 | ISOW | Sedigraph |
| ODP983, MIS 18-22 | RMA Gp 1 | 24.09 | 16.07 | 0.149 | 12.47 | 0.888 | 358 | ISOW | Sedigraph |
| ODP983, MIS 18-22 | RMA Gp 2 | 39.81 | 20.07 | 0.188 | 12.57 | 0.736 | 81 | ISOW | Sedigraph |
| **Other Locations** | | | | | | | | | |
| HLY501-05JPC | RMA (-3 outliers) | 3.37 | 11.00 | 0.177 | 10.41 | 0.960 | 27 | Beaufort slope C. | Coulter |
| AMD0214-02PC | RMA all | 10.98 | 12.23 | 0.190 | 10.15 | 0.899 | 33 | Chukchi slope C. | Coulter |
| MR806-PC09 | RMA all | 48.17 | 27.54 | 0.387 | 8.92 | 0.914 | 68 | ACC | Coulter |
| MD07-3128 | all | | | 0.191 | 7.80 | 0.825 | 218 | ACC/CHornCurr | Sedigraph |
| ANT30/PC-01 | lin regr all | | | 0.071 | 17.30 | 0.465 | 312 | Ant Slope Curr | Coulter |
| ANT30/PC-01 | RMA: Ehol, T-II,T-III | 30.35 | 19.46 | 0.216 | 12.90 | 0.949 | 27 | Ant Slope Curr | Coulter |
| ANT30/PC-01 | RMA: T-IIIa,T-V,T-VIa | 30.65 | 18.47 | 0.083 | 15.94 | 0.855 | 19 | Ant Slope Curr | Coulter |
| ANT30/PC-01 | RMA glacials R>0.9 | 23.62 | 19.48 | 0.153 | 15.86 | 0.778 | 82 | Ant Slope Curr | Coulter |
| **Other data** | | | | | | | | | |
| HU70037-surface | RMA all (-1outlier) | 65.94 | 24.92 | 0.350 | 1.83 | 0.961 | 56 | WGC | Malvern |
| Jia Loess | RMA | | | 0.240 | 10.55 | 0.776 | 150 | | Coulter |
| Xu et, Miss Delta top | all | | | 0.093 | 21.91 | 0.211 | 93 | | Coulter |
| Gammon, Lake | all | | | 0.138 | 14.83 | 0.493 | 701 | | Coulter |
| Gammon, lake | RMA (SS%>62.5) | | | 0.220 | 7.57 | 0.819 | 109 | | Coulter |